

**3D PRINTING PLA-GRAPHENE OXIDE NANOCOMPOSITES USING
IN-SITU FUSED DEPOSITION MODELING**

BY

TARIG YASSIN MAKKI

A Thesis Presented to the
DEANSHIP OF GRADUATE STUDIES

KING FAHD UNIVERSITY OF PETROLEUM & MINERALS

DHAHRAN, SAUDI ARABIA

In Partial Fulfillment of the
Requirements for the Degree of

MASTER OF SCIENCE

In

MECHANICAL ENGINEERING

December 2023

KING FAHD UNIVERSITY OF PETROLEUM & MINERALS

DHAHRAN- 31261, SAUDI ARABIA

DEANSHIP OF GRADUATE STUDIES

This thesis, written by Tarig Yassin Makki under the direction of his thesis advisor and approved by his thesis committee, has been presented and accepted by the Dean of Graduate Studies, in partial fulfillment of the requirements for the degree of **MASTER OF SCIENCE IN MECHANICAL ENGINEERING.**



Dr. Usman Ali
(Advisor)



Dr. Mohamed Antar
Department Chairman



Dr. Awad Alquaity
(Member)



Dr. Suliman Al-Homidan
Dean of Graduate Studies



Dr. Ahmed Sarhan
(Member)

Date



© Tarig Yassin Makki

2023

My thesis is dedicated to my family for their unwavering support and endless encouragement throughout my academic journey. I am profoundly grateful for their sacrifices, understanding, and constant motivation, without which this achievement would have not been possible.

ACKNOWLEDGMENTS

My heartfelt appreciation goes out to KFUPM and the IRC for Advanced Materials at KFUPM for their invaluable financial support throughout my academic journey. Additionally, I am immensely grateful to my thesis supervisor, Dr. Usman Ali. Your unwavering commitment to academic excellence, your profound knowledge in the field, and your continuous guidance have been instrumental in shaping this thesis. Your mentorship has not only enhanced my understanding of the subject matter but has also fostered my growth as a researcher.

I express my deepest gratitude to Dr. Rajesh and Mr. Abdulazeem for their invaluable contributions and insightful feedback. Their expertise, critical analysis, and constructive suggestions have significantly enriched the quality and depth of this research. I would also like to extend my genuine appreciation to my thesis committee members, Dr. Awad Alquaity and Dr. Ahmed Sarhan.

Lastly, I would like to highlight my heartfelt gratefulness to my family, friends, and loved ones for their unwavering support and encouragement. Their belief in my abilities and their constant motivation have been the driving force behind my success.

TABLE OF CONTENTS

ACKNOWLEDGMENTS	V
TABLE OF CONTENTS	VI
LIST OF TABLES	VIII
LIST OF FIGURES	IX
LIST OF ABBREVIATIONS	XI
ABSTRACT	XII
ملخص الرسالة.....	XIII
1 INTRODUCTION	1
1.1 Background	1
1.2 Motivation.....	3
1.3 Thesis objectives	3
1.4 Methodology	4
2 LITERATURE REVIEW	5
2.1 Steps in AM	5
2.2 Types of AM processes	6
2.2.1 Fused deposition modeling (FDM).....	6
2.2.2 Binder jetting (BJ)	7
2.2.3 Stereolithography (SLA)	7
2.2.4 Laser powder-bed fusion (LPBF)	8
2.2.5 Laminated object manufacturing (LOM).....	9
2.2.6 Directed energy deposition (DED)	10
2.2.7 Material jetting (MJ).....	11
2.3 Materials used in AM.....	12
2.4 AM main applications	13
2.4.1 Biomedical.....	13
2.4.2 Automotive	14
2.4.3 Aerospace	14
2.4.4 Electronics	14
2.4.5 Construction	15
2.5 Fused deposition modeling (FDM)	15
2.5.1 FDM material properties	17
2.5.2 FDM process parameters	19
2.5.3 FDM composites	20
2.5.4 FDM composite preparation methods	21

2.5.5	Graphene based FDM studies.....	25
3	EXPERIMENTAL METHODOLOGY	29
3.1	Scanning electron microscopy (SEM)	31
3.2	Thermogravimetric analysis (TGA).....	32
3.3	Differential scanning calorimetry (DSC).....	33
3.4	X-ray diffraction (XRD)	33
3.5	Fourier transform infrared spectroscopy (FTIR).....	34
3.6	Tensile, compressive, and flexural test	35
3.7	Impact test.....	36
3.8	Hardness and micro-hardness	37
4	RESULTS AND DISCUSSION	38
4.1	Scanning electron microscope (SEM).....	38
4.2	Thermogravimetric analysis (TGA).....	39
4.3	Differential scanning calorimetry (DSC)	42
4.4	X-ray diffraction (XRD)	45
4.5	Fourier transform infrared spectroscopy (FTIR).....	46
4.6	Tensile test	48
4.7	Tensile fracture surface.....	51
4.8	Compression test.....	53
4.9	Flexural test	55
4.10	Impact test.....	58
4.11	Hardness test.....	60
5	CONCLUSIONS	63
	REFERENCES	66
	VITAE.....	90

LIST OF TABLES

Table 2.1: Materials utilized in AM [51].	13
Table 2.2: FDM pure polymer properties	18
Table 2.3: Publications on FDM PLA-graphene	26
Table 3.1: Selected FDM process parameters.....	30
Table 4.1: TGA results for PLA and PLA-GO	41
Table 4.2: FDM PLA and PLA-GO DSC results	44

LIST OF FIGURES

Figure 2.1 AM process flowchart	5
Figure 2.2: Fused Deposition Modeling (FDM) [28]	6
Figure 2.3: Binder Jetting (BJ) [32].....	7
Figure 2.4: Stereolithography (SLA) [35]	8
Figure 2.5: Selective laser sintering/melting (SLS/SLM) [38].....	8
Figure 2.6: Laminated object manufacturing (LOM) [43].....	10
Figure 2.7: Directed energy deposition (DED) [46]	11
Figure 2.8: Material Jetting (MJ) [50]	12
Figure 2.9: Fused Deposition Modeling setup (FDM).....	16
Figure 2.10: The history of FDM [15]	17
Figure 2.11: FDM process parameters [84]	20
Figure 2.12: In composite filaments, a variety of reinforcing materials are used; (i) Particulate reinforcement (ii) Short fiber reinforcement (iii) Continuous fiber reinforcement.....	21
Figure 2.13: Solution mixing [87]	22
Figure 2.14: Direct mixing via extrusion.....	23
Figure 2.15: FDM in-situ [86]	24
Figure 3.1: FDM nanocomposite preparation method.....	30
Figure 3.2: Dimensions of PLA and PLA-GO samples for; (a) Tensile tests, (b) Flexural tests (c) Compression tests, (d) Impact tests	31
Figure 3.3: SEMoscope IEM11+	32
Figure 3.4: TA Instruments SDT Q600 TGA machine.....	32
Figure 3.5: (DSC) Q2000 V24.9 TA instruments® machine	33
Figure 3.6: Rigaku® Mini Flex II XRD machine.....	34
Figure 3.7: Nicolet iS10 FTIR machine.....	34
Figure 3.8: (a) Instron® 3367 Universal Test System tensile test setup (b) Instron® 5569 Universal Test System compression test setup (c) Instron® 3367 Universal Test System flexural test setup.....	36
Figure 3.9: gunt® WP 400 Impact test machine.....	36

Figure 3.10: (a) Tinius Olsen hardness test machine (b) Nextgen Micro Vickers hardness machine	37
Figure 4.1: (a) PLA and PLA-GO samples SEM images of (b) PLA, (c) PLA-GO	39
Figure 4.2: FDM PLA-GO SEM images	39
Figure 4.3: TGA curves for FDM PLA and PLA-GO	41
Figure 4.4: PLA and PLA-GO DSC curves.....	43
Figure 4.5: The effect of graphene on the crystallinity of PLA.....	44
Figure 4.6: PLA and PLA-GO XRD results	45
Figure 4.7: FTIR results for FDM PLA and PLA-GO.....	48
Figure 4.8: (a) Tensile- stress vs strain curves, (b) Tensile strength (TS) (c) Tensile modulus, (d) Reduction in area (e) Elongation at break.....	50
Figure 4.9: SEM Fracture surfaces, (a) PLA, (b) PLA-GO	53
Figure 4.10: (a) Compression stress vs strain curves, (b) Compressive strength, (c) Compressive modulus, (d) Compressive yield stress	54
Figure 4.11: Flexural test results for PLA and PLA-GO samples (a) Force vs Displacement curves, (b) Flexural strength, (c) Flexural modulus.....	56
Figure 4.12: Fracture surface of flexural samples, (a) Top surface, (b) Bottom surface..	58
Figure 4.13: Impact test results	59
Figure 4.14: (a) Rockwell-R hardness results and (b) Vickers micro hardness test results	61
Figure 4.15: Dispersion of graphene in PLA (a) Agglomerated, (b) Uniform dispersion	62

LIST OF ABBREVIATIONS

ABS	:	Acrylonitrile butadiene styrene
AM	:	Additive manufacturing
BJ	:	Binder jetting
CAD	:	Computer Aided Design
DED	:	Directed energy deposition
DSC	:	Differential Scanning Calorimetry
EBM	:	Electron beam melting
FDM	:	Fused deposition modelling
FTIR	:	Fourier Transform Infrared Spectroscopy
LPBF	:	Laser powder-bed fusion
PC	:	Polycarbonate
PLA	:	Polylactic acid
SEM	:	Scanning electron microscope
SLA	:	Stereolithography
SLS/ SLM	:	Selective laser sintering/melting
TGA	:	Thermogravimetric analysis
TS	:	Tensile strength
YS	:	Yield strength
XRD	:	X-ray Diffraction

ABSTRACT

Full Name : Tarig Yassin Makki
Thesis Title : 3D printing PLA-graphene oxide nanocomposites using in-situ Fused Deposition Modeling
Major Field : Mechanical Engineering
Date of Degree : December 2023

This dissertation focusses on fused deposition modeling (FDM) and its crucial role in the fabrication of Polylactic Acid (PLA) alongside PLA-graphene oxide (GO) composites. The study aims to study the manufacturing, understanding, and utilization of these materials, with the objective of enhancing the adaptability and capabilities of FDM technology. Commencing with an analysis of PLA, this research aims to explore the advantages, and limitations within the context of 3D printing using FDM. Subsequent investigations involve the integration of graphene oxide into the PLA matrix using an in-situ nozzle impregnation technique. This amalgamation seeks to bolster PLA's fundamental characteristics, thereby fostering enhancements in its mechanical and thermal characteristics. To evaluate the manufactured the FDM PLA and PLA-GO nanocomposites, various characterization methodologies were utilized along with tensile, compression, flexural, impact, and hardness tests. The findings of this thesis shed light on the improvement in the mechanical and thermal properties of FDM PLA parts with the addition of GO.

ملخص الرسالة

الاسم الكامل: طارق ياسين مكي

عنوان الرسالة: تصنيع مركبات الأحماض البوليلاتيك - أكسيد الغرافين باستخدام طباعة ثلاثية الأبعاد ونمذجة الترسيب المنصهرة في الموقع

التخصص: الهندسة الميكانيكية

تاريخ الدرجة العلمية: ديسمبر ٢٠٢٣

تركز هذه الرسالة على نمذجة الترسيب المنصهرة والدور الحيوي الذي تلعبه في تصنيع حمض البوليلاتيك بجانب مركبات حمض البوليلاتيك - أكسيد الغرافين. تهدف الدراسة إلى دراسة تصنيع وفهم واستخدام هذه المواد، بهدف تعزيز قابلية التكيف والقدرات لنمذجة الترسيب المنصهرة. بدايةً مع تحليل حمض البوليلاتيك، تهدف هذه البحث إلى استكشاف المزايا والقيود في سياق الطباعة ثلاثية الأبعاد باستخدام نمذجة الترسيب المنصهرة. تشمل الاستقصاءات اللاحقة دمج أكسيد الغرافين في مصفوفة حمض البوليلاتيك باستخدام تقنية الامتصاص بالفوهة في الموقع. يسعى هذا التوحيد إلى تعزيز الخصائص الأساسية لحمض البوليلاتيك، مما يعزز من خصائصها الميكانيكية والحرارية. لتقييم نمذجة الترسيب المنصهرة لحمض البوليلاتيك ومركبات حمض البوليلاتيك - أكسيد الغرافين النانوية المصنعة، تم استخدام منهجيات توصيف متنوعة بالإضافة إلى اختبارات الشد والضغط والانتشاء والصدمات والصلادة. تسلط نتائج هذه الأطروحة الضوء على التحسين في الخصائص الميكانيكية والحرارية لقطع نمذجة الترسيب المنصهرة لحمض البوليلاتيك مع إضافة أكسيد الغرافين.

CHAPTER 1

INTRODUCTION

1.1 Background

AM is embraced across industries for its transformative impact. Its widespread adoption is fueled by various factors such as its unique capacity for unrestricted design [1]. Unlike traditional methods constrained by machining, it enables the creation of intricate geometries, empowering engineers to optimize parts for better performance and appearance [2]. Other than design freedom, efficiency in cost and waste reduction is another driving force behind the widespread acceptance and adoption of AM. This approach streamlines inventory management and significantly reduces material costs [3]. Over the last couple of decades, AM has undergone a staggering amount of development. [4]

Numerous AM techniques, including SLA [4], (SLS) [5], FDM [6], and so forth, have emerged due to the development of AM technologies. Among the various 3D printing methods available, FDM is considered the most utilized AM process due to its low cost compared to other AM processes. In recent years, FDM has expanded quickly across an array of trades, such as the automotive, aerospace, electronics, and biomedical sectors [7]–[10].

Researchers have used several materials for FDM such as PLA, PC, and ABS, however PLA stands out as the most utilized polymer in FDM owing to several factors, notably its biodegradability [11]. PLA's biodegradation occurs when exposed to oxygen and UV light, distinguishing it from other polymers. PLA offers minimal posing a minimal

environmental hazard as it decomposes into carbon dioxide and water [12]. The notable advantages of this thermoplastic filament in 3D printing encompass its user-friendly nature and exceptional dimensional precision [13]. Nonetheless, PLA faces limitations in its applications due to its relatively low strength and resistance to heat.

Predicting the mechanical behavior of manufactured parts subjected to external loads is essential to any engineering design and is the biggest barrier for FDM parts [14]. In order to improve the properties, researchers have tried to add various additives to increase part strength. In comparison to the pure polymer, the properties of the reinforced polymers are improved by nanoparticles, short fibers, or continuous fibers [15]. To identify the crucial aspects of the FDM process and the characteristics of the filaments used as the feedstock, further research must be carried out in the future [16].

As discussed previously, researchers have used several fillers to improve the performance of conventional FDM materials [17], [18]. The fillers are added to FDM filaments by using either direct mixing or solution mixing techniques [20]–[24]. Due to its superior mechanical properties, graphene oxide (GO) has also been used by researchers as a nanofiller to improve the properties of FDM parts [19]–[23]. Belaid et al. [19] used graphene oxide to improve the TS (by 14%) of PLA by mixing the solutions and extruding a PLA-GO filament. Zhang et al. [20] generated FDM PLA-GO flexible circuits by solution mixing and melt blending via a twin-screw extruder resulting in improved TS and modulus. Chen et al. [22] conducted a similar study, with a PLA/TPU copolymer and showed a 90% increase in the TS of FDM PLA/TPU-GO parts. However, in all the studies, the elongation at break diminished due to an increase in TS and stiffness [19], [20].

1.2 Motivation

While FDM offers design flexibility, parts produced may have weaker mechanical characteristics. For instance, compared to parts from traditional manufacturing methods like CNC machining or injection molding, FDM parts have lower strength and toughness due to the layered deposition process [17]. As nanofillers can improve the part performance of FDM parts, this work investigates the effect of GO nanofiller on the mechanical, thermal, and molecular behavior of FMD PLA parts. In addition, unlike the conventional method discussed previously, this work uses a novel in-situ nozzle impregnation method where PLA is combined with the GO filler during manufacturing.

1.3 Thesis objectives

This thesis focuses on the effect of using GO as a nanofiller for FDM-PLA parts. The objectives of this thesis are as follows:

- I. Manufacture 3D printed/additively manufactured (AM) FDM PLA and PLA-GO parts with in-situ nozzle impregnation technique with varying layer heights
- II. Characterize the FDM PLA and PLA-GO parts for mechanical, thermal, and morphological properties.
- III. Analyze the PLA and PLA-GO part performance under uniaxial tension, compression, flexural and impact loading
- IV. Characterize the fracture behavior of FDM PLA and PLA-GO parts
- V. Assess the importance of PLA-graphene oxide composites for FDM applications, facilitating advancements in additive manufacturing processes.

1.4 Methodology

The primary objective of this thesis is to investigate and characterize the influence of GO as a nanofiller on the mechanical and thermal behavior of FDM-PLA. The preparation of FDM PLA-GO composites involved thorough mixing and homogenization of the graphene oxide to ensure uniform dispersion in the PLA matrix. FDM process with optimal process parameters were employed to manufacture various PLA and PLA-GO test specimens with varying layer heights.

DSC was employed to analyze thermal transitions of PLA and PLA-GO parts. TGA was used to investigate thermal stability and decomposition behavior of the FDM samples. Similarly, XRD and FTIR were employed for identification of crystalline phases and chemical composition/bonding.

The FDM PLA and PLA-GO samples with varying heights were also characterized to understand their tensile, compression, bending, impact, and hardness properties according to ASTM standards. Tensile and bending fracture mechanisms were also evaluated. The experimental data was analyzed statistically to discern trends and correlations. In addition, comparative analyses were conducted to comprehend the impact of GO as a nanofiller.

The inclusion of the work performed in this dissertation aims to provide a thorough interpretation of the morphological, structural, and chemical aspects of the FDM nanocomposites, complementing the mechanical and thermal property analyses. The outcomes of this research are expected to contribute valuable insights into optimizing the formulation of PLA-graphene composites for FDM applications, facilitating advancements in additive manufacturing processes.

CHAPTER 2

LITERATURE REVIEW

2.1 Steps in AM

AM processes possess a sequence of crucial steps to produce three-dimensional objects as shown in Figure 2.1 [24]. It starts with designing a digital model using CAD software, serving as a detailed blueprint for the printing process. Special software then divides the digital model into thin layers, generating instructions (G-code) for the printer. Parameters like layer height, nozzle speed and temperature are adjusted to achieve the desired quality. Choosing the appropriate material for the desired application and preparing it for printing is crucial. The 3D printer then interprets instructions and constructs the object layer-by-layer. Post-printing processes, such as removing supports or refining surfaces, may be required. Finally, a thorough quality check ensures the printed object meets specifications. Together, these steps enable the creation of precise and customized objects applicable across various industries.

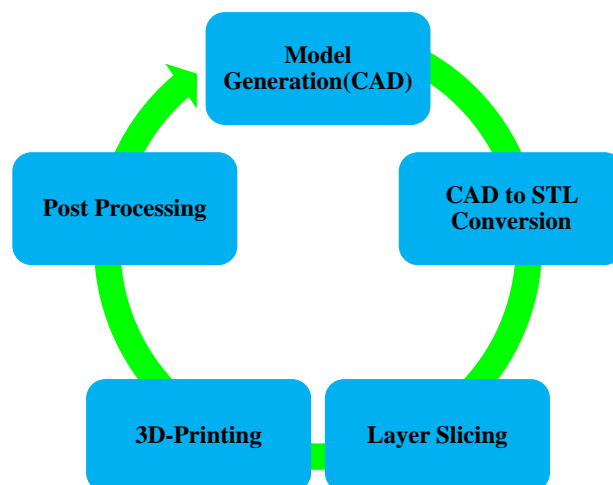


Figure 2.1 AM process flowchart

2.2 Types of AM processes

This section highlights the various AM technologies classified by the type of feedstock and the bonding method. There are seven types of AM processes, and they are discussed in detail below.

2.2.1 Fused deposition modeling (FDM)

FDM (Figure 2.2) is used in this work and is the most common method for manufacturing polymer parts [25]. A moveable FDM head is used to extrude threads of molten polymer thermoplastic, which is then deposited in a layer-by-layer fashion and solidified to create finished parts. Polymers such as PLA and ABS are frequently utilized in this technique. Numerous FDM process parameters, including the printing orientation, layer height and raster angle can be altered to regulate the quality of printed objects [26]. Although FDM has significant drawbacks, such as poor surface quality, slow manufacturing process, and delamination, FDM parts are employed in industries such as the automotive, medical, electronics etc. [27].

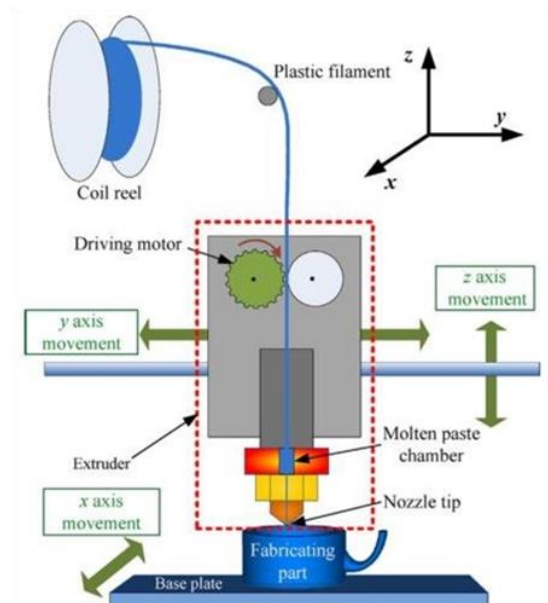


Figure 2.2: Fused Deposition Modeling (FDM) [28]

2.2.2 Binder jetting (BJ)

Binder Jet printing (Figure 2.3) is a form of AM where liquid binding agents are applied to layers of powder to create a specific pattern [29]. These layers are then stacked to form a physical object. This method is adaptable to different materials such as polymers, metals etc. In addition, binder jetting allows for high production rates and utilizing various technologies such as printing techniques, powder deposition, binder-powder interactions, and post-processing methods [30]. It has been successful in processing a wide array of materials like polymers, metals, and ceramics [31].

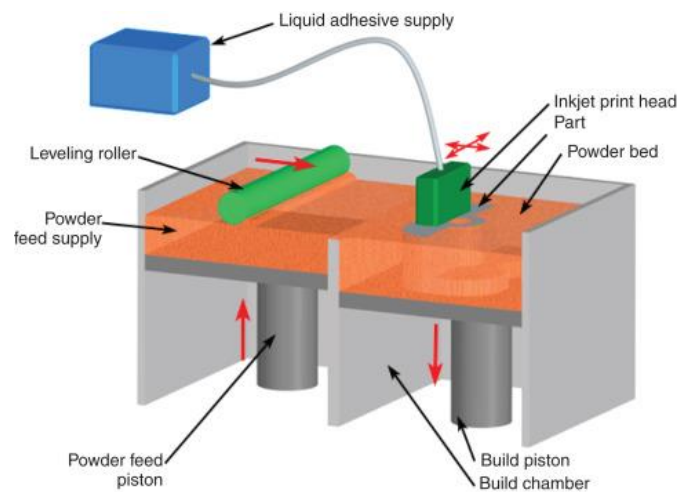


Figure 2.3: Binder Jetting (BJ) [32]

2.2.3 Stereolithography (SLA)

In SLA (Figure 2.4), a polymeric resin chain reaction is started using UV light or an electron beam [33]. Selective layer-by-layer UV curing of resin is used to manufacture parts [34]. Materials like acrylic and epoxy polymers are frequently employed. SLA printed parts are exposed to post processing procedures, such as heating, to give them the necessary physical performance. The need for post-processing and a limited build volume are some of the drawbacks of SLA [27].

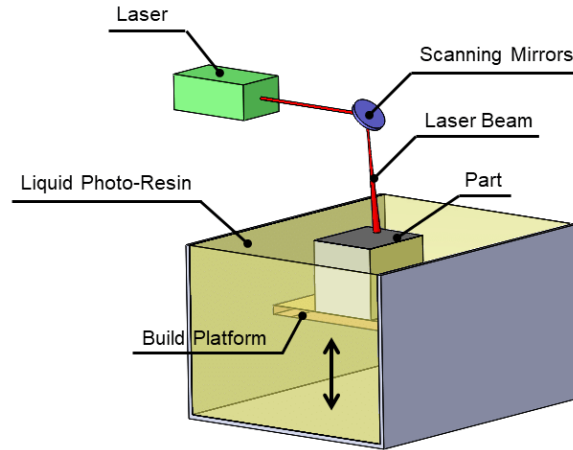


Figure 2.4: Stereolithography (SLA) [35]

2.2.4 Laser powder-bed fusion (LPBF)

LPBF is divided into SLS and SLM processes (Figure 2.5). In SLS, process polymers are used as the feedstock while metals are used in SLM [36]. In the LPBF approach, small polymer/metal particles are fused together using a laser source. To create 3D parts, the laser scans the powder-bed layer-by-layer [27]. To promote the fusing of several layers and avoid thermal deformation, the powder is heated just below its melting point [37]. Unbounded powder is removed from the finished product to obtain the final part. Only a few polymers, including polyamide, polyethylene, polycaprolactone, and polyetheretherketone, are used in SLS [27].

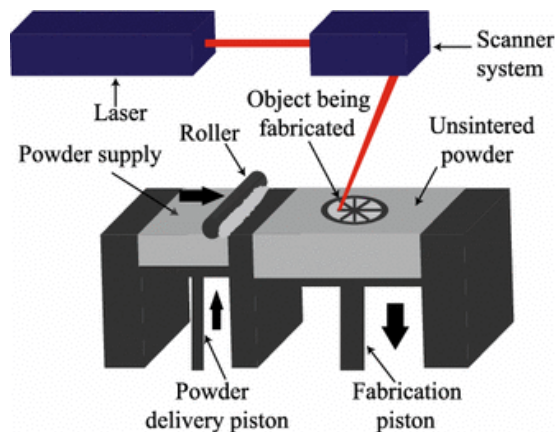


Figure 2.5: Selective laser sintering/melting (SLS/SLM) [38]

In SLM, construction begins by spreading a thin metal powder layer onto a base plate within a construction area [39]. A highly concentrated laser then melts and merges specific sections based on the programmed instructions. Once the laser completes its scan, the base is lowered, a fresh powder layer is added, and the laser scans it for the next layer. This cycle repeats for subsequent layers until the desired components are fully formed [39]. An electron beam could also be utilized to melt and fuse the metal powders in a similar AM process known as electron beam melting (EBM) [40].

2.2.5 Laminated object manufacturing (LOM)

In LOM (Figure 2.6) successive layers of paper sheets covered with adhesive are bonded and laser-cut to manufacture a 3D part [41]. The build material is presented either on a roll or in the form of sheet stock, and pressure is increased to enhance the interlayer bonding using a heated platen or a moving roller. The melting and fusion of thermoset or thermoplastic polymers that permeate the fiber allows LOM of composite materials to permit interlayer bonding [42]. The use of CNC milling and room-temperature metal deposition in tandem is encouraged by a subclass of LOM known as ultrasonic additive manufacturing (UAM). LOM's primary distinguishing characteristic is its ability to generate complex 3D components with less manufacturing and post-processing expense in comparison to other AM processes [35].

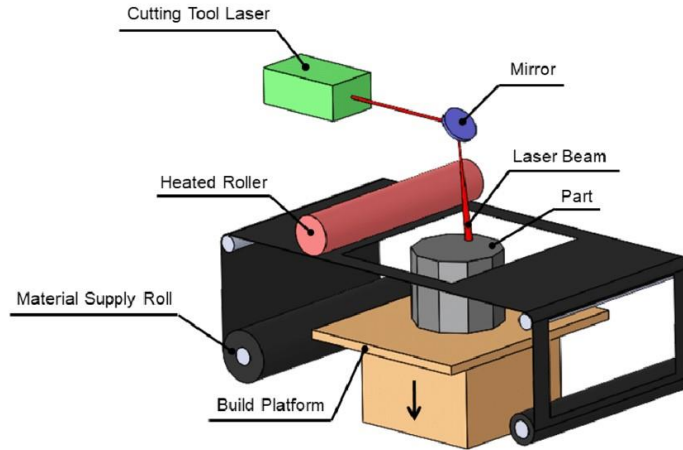


Figure 2.6: Laminated object manufacturing (LOM) [43]

2.2.6 Directed energy deposition (DED)

DED (Figure 2.7) is carried out by concentrating a laser beam on the build platform while simultaneously feeding with a stream of powders [44]. To prevent the formation of oxides and undesired alloying, an inert gas is pumped between the laser beam and the powder stream [35]. Instead of employing a powder-bed, Directed Energy Deposition (DED) uses a power source, such as a laser, electric arc, or electron beam, to deposit and create 3D objects out of wire (wire-fed) or powder (powder-fed). The difference between powder and wire-fed DED systems lies in the supply system. DED has better flexibility and buildup rate compared to LPBF and is encouraged to have an unrestricted build envelope [45].

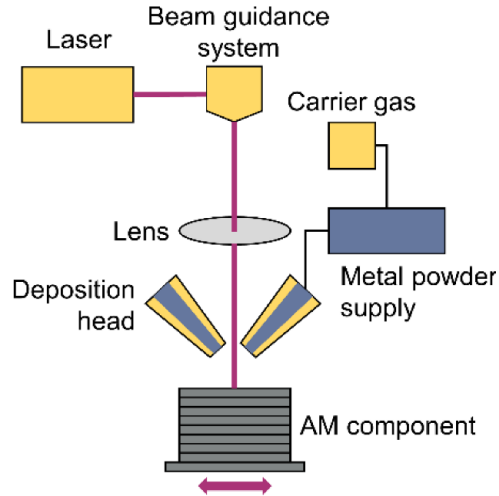


Figure 2.7: Directed energy deposition (DED) [46]

2.2.7 Material jetting (MJ)

In the MJ process (Figure 2.8) specialized tanks hold photopolymer substances, dispensed as small droplets, forming precise layers on the build platform [47]. Before reaching the nozzle, the photopolymer undergoes heating along a transmission line. Subsequently, ultraviolet (UV) light is directed onto the liquefied material on the build platform, initiating the curing process. This technique employs a specific UV wavelength to solidify the liquid monomers or oligomers, a process termed photopolymerization or photo-curing [48]. Once each layer is cured, the build platform descends by a defined thickness, and fresh liquid material is sprayed onto the preceding layer. This cycle continues, curing each new layer until a complete part is entirely fabricated [49].

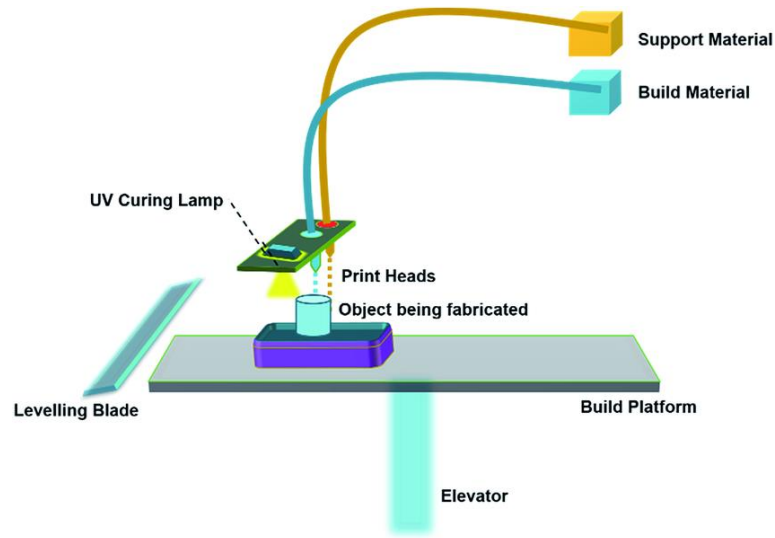


Figure 2.8: Material Jetting (MJ) [50]

2.3 Materials used in AM

Additive manufacturing (AM) materials are typically classified into polymers, ceramics, and metals. Among these, polymers have historically been used frequently due to their widespread accessibility and ease of handling. However, innovations in technology allow for the production of materials other than typical polymers, resulting in a wider choice of options. While polymeric materials have been the main focus in 3D printing, recent progress has enabled the printing of not just diverse polymers but also metals and ceramics. This evolution has made 3D printing a highly adaptable manufacturing choice. The elementary materials (polymers, ceramics, and metals) each offer distinct uses, advantages, and challenges in additive manufacturing. These key characteristics for each material category are succinctly outlined in Table 2.1, providing a clear summary of their applications and attributes within the additive manufacturing field.

Table 2.1: Materials utilized in AM [51].

Materials	Main Applications	Benefits	Challenges
Metals and alloys	Aerospace and Automotive Military Biomedical	Multifunctional optimization Mass-customization Reduced material waste Fewer assembly components Possibility to repair damaged or worn metal parts	Limited selection of alloys Dimensional inaccuracy and poor surface finish Post-processing may be required (machining, heat treatment or chemical etching)
	Aerospace and Automotive Sports Medical Architecture Toys Biomedical	Fast prototyping Cost-effective Complex structures Mass-customisation	Weak mechanical properties Limited selection of polymers and reinforcements Anisotropic mechanical properties (especially in fibre-reinforced composites)
Ceramics	Biomedical Aerospace and Automotive Chemical industries	Controlling porosity of lattices Printing complex structures and scaffolds for human body organs Reduced fabrication time A better control on composition and microstructure	Limited selection of 3D-printable ceramics Dimensional inaccuracy and poor surface finish Post-processing (e.g., sintering) may be required Layer-by-layer appearance
	Concrete	Infrastructure and construction	Anisotropic mechanical properties Poor inter-layer adhesion Difficulties in upscaling to larger buildings Limited number of printing methods and tailored concrete mixture design

2.4 AM main applications

Additive manufacturing (AM) finds widespread applications across various industries, including biomedical [52], automotive [53], aerospace [54], electronics [55], and construction [56]. In these diverse sectors, AM plays a pivotal role in advancing production methods and enhancing efficiency. This section will discuss the main applications of AM in detail to help in conveying the importance of AM.

2.4.1 Biomedical

Some of the most inventive and promising applications of AM can be found in the medical profession. Bioprinting, a cutting-edge technique, allows for the accurate molecular creation of human tissues derived from stem cells [57]. This technique has aided in the development of personalized prostheses, specialized drug delivery systems, scaffolds

essential for tissue engineering, and implants [58]. To ensure compatibility with the body, additive manufacturing utilizes polymers, metals, and ceramics, often integrating different enhancing agents [51].

2.4.2 Automotive

AM parts are utilized in the automotive industry by allowing quick prototyping, customization, and the production of intricate, lightweight parts [59], [60]. F1 gearboxes, MotoGP air boxes, dashboards, camshaft covers, and suspension systems are being manufactured using various AM systems [10]. In the automotive industry, the use of AM has led to notable advantages, such as a 20%-25% weight reduction, about 20% less volume, twice the torsion stiffness for F1 gearboxes, reduced gear wear, and lower power consumption compared to conventional manufacturing methods [10].

2.4.3 Aerospace

Additive manufacturing (AM) is reshaping various sectors in the aerospace field [61], spanning commercial and military aircraft, space exploration, and missile systems [62]. The aerospace industry has adopted AM technologies by integrating numerous parts, including exclusive nonmetallic elements. For example, Boeing's venture into titanium AM parts foresees substantial per-aircraft cost reductions [63]. Similarly, GE Aviation's use of metal AM to build numerous fuel nozzles for the LEAP engine each year demonstrates the technology's importance in aerospace [62].

2.4.4 Electronics

3D-Printed electronics play a substantial role in electronics manufacturing, offering benefits in large-scale production and adaptability in material support and system processes

[64]. Additive manufacturing research is increasingly concentrating on printing components like traces, interconnects, passive elements (such as resistors and capacitors), and specialized electronic devices [65]. Furthermore, when conductive substances are used, AM composites can be deployed as electrical devices, including an array of sensors such as piezo resistive and capacitive sensors created using AM techniques [66].

2.4.5 Construction

Additive manufacturing is witnessing global growth, notably in the construction domain [51]. This technology enables continuous construction from a distance, utilizing materials like concrete, glass, metal, and wood [67]. Large-scale 3D printers are crucial for building structures and infrastructure, as they can swiftly solidify concrete in substantial amounts [68]. Unlike traditional construction processes, which require specialized individuals to prepare concrete, which is time-consuming and expensive, 3D printers continuously manufacture materials for each stage of the project. This feature allows people in the construction sector to manage multiple projects concurrently using a single 3D printer, resulting in significant savings in time and expenditure [51].

2.5 Fused deposition modeling (FDM)

The growth of FDM owes its advancement to the emergence of affordable home printers introduced by pioneering companies like MakerBot® and Ultimaker®. Presently, there is a widespread presence of FDM printers, with over a hundred manufacturers and distributors worldwide [69]. The FDM setup (Figure 2.9) consists of four main components. A heated printing bed is used to help printed layers adhere to each other. The extruder pushes and melts the filaments on the heated bed to build the model. Moreover,

there are moving parts in the FDM machine that move the heated bed and extruder in X, Y and Z-axis.

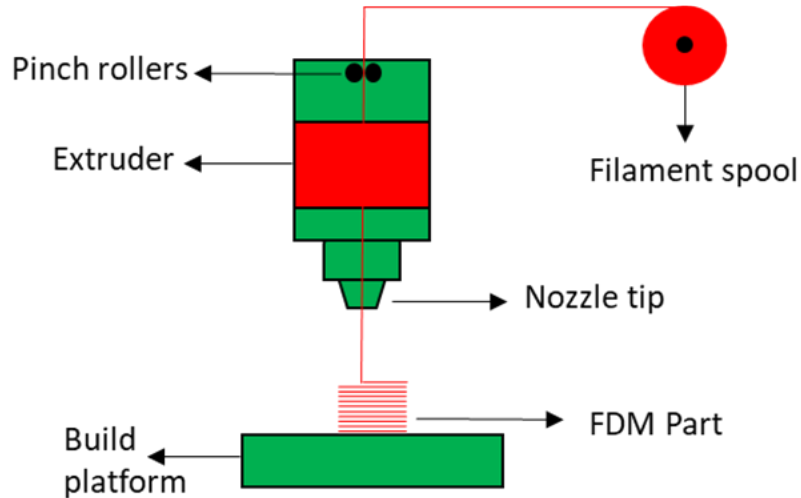


Figure 2.9: Fused Deposition Modeling setup (FDM)

FDM, known for its versatility using filament feedstock and moderate melting temperature, primarily focuses on thermoplastic polymers and their composites [15]. Traditionally, it relied on amorphous polymers, notably ABS and PLA, mainly for prototypes, not suitable for critical components needing high strength and stiffness. However, continued FDM advancements have resulted in the generation of diverse polymeric materials and composites, allowing the creation of functional parts [70], [71]. Figure 2.10 outlines the key milestones in FDM technology. The relationship between materials and processes underscores the importance of considering FDM feedstock and process parameters for achieving practical 3D printed parts.

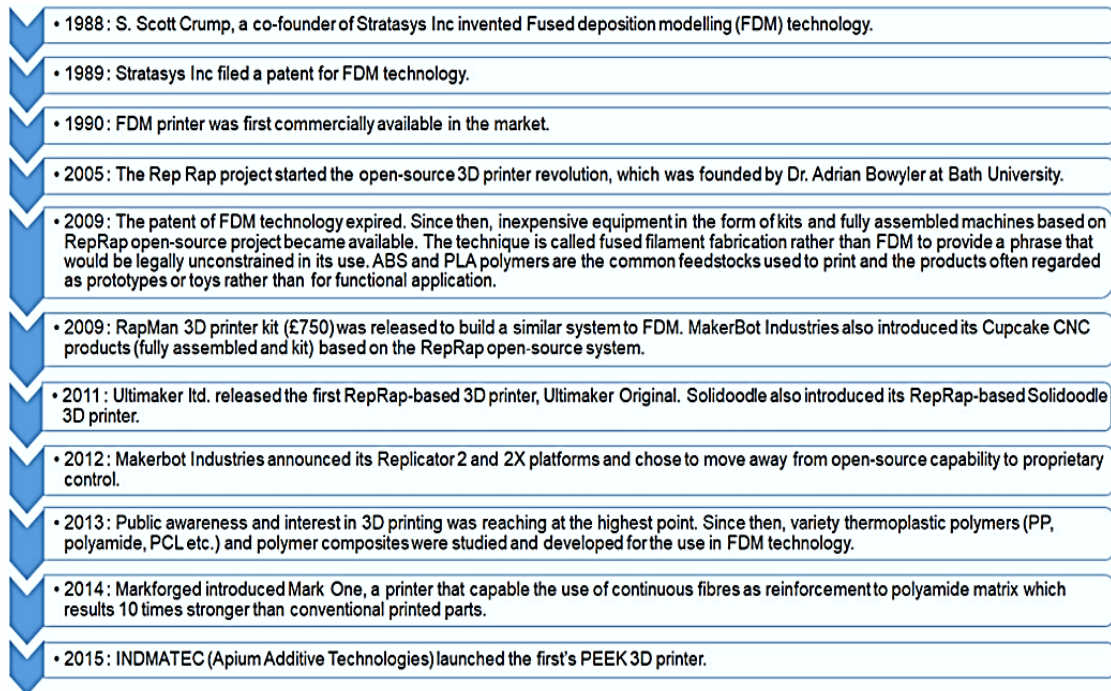


Figure 2.10: The history of FDM [15]

2.5.1 FDM material properties

This section offers a broad overview of the mechanical, thermal, and physical characteristics of the various thermoplastics utilized in the production of FDM filaments. Being a polymer-based process, FDM process dictates certain criteria for the raw filaments used for manufacturing. The polymer's amorphous or semi-crystalline structure and their respective crystallization temperatures affect the FDM process [17]. Amorphous polymers are well suited for FDM printing due to their rapid solidification, resulting in minimal shrinkage [72]. This swift solidification is also crucial for layer adherence. However, it might take longer to print semi-crystalline polymers due to their high crystallinity and cooling rates [17]. The crystalline structures also lead to increased shrinkage and potential distortion of printed parts, making them less suitable for FDM. Table 2.2 presents a summary of these materials and their respective properties. PEEK shows the highest melting temperature (343°C) and glass transition temperature (143°C). These attributes

pose significant challenges for FDM production using commonly available machines, resulting in the rare utilization of PEEK. Additionally, PEEK exhibits the highest heat deflection temperature (156°C), signifying its suitability for use in high-temperature applications.

Contrarily, widely employed FDM materials like ABS and PLA feature a melting temperature around 200°C, allowing their accommodation on most FDM machines. Amorphous polymers such as ABS lack a distinct melting point; instead, they tend to transition from a glassy state as they approach the glass transition temperature [73].

Table 2.2: FDM pure polymer properties

Polymer	Thermoplastic Type	Melting temperature (°C)	Glass transition temperature (°C)	Density (g/cm ³)	Melt-mass flow rate * (g /10 min)	Heat deflection Temperature (°C)
PLA [74]	Semi-crystalline	152	59.1	1.24	6.1	58.8
ABS [75]	Amorphous	-	101	1.1	41	86.6
PVA [76]	Semi-crystalline	175	58.4	1.23	17	-
PEEK [77]	Semi-crystalline	343	143	1.3	-	156
PETG [78]	Amorphous	-	77.4	1.27	6.2	76.2
NYLON [79]	Semi-crystalline	188	55.1	1.14	6.2	89.2
PP [80]	Semi-crystalline	131	-	0.89	20	64.1
PET [81]	Amorphous	-	71	1.33	16.3	63
PC [82]	Amorphous	-	111	1.18	32	111
TPU [83]	Semi-crystalline	217	-	1.22	15.9	50.3

*The melt-mass flow rate is conducted at 225 °C, 1.2 kg.

2.5.2 FDM process parameters

The FDM process parameters are chosen to optimize part performance, based on the material properties (Figure 2.11). Build orientation refers to the positioning of the part concerning the X, Y, and Z axes on the build platform. The X and Y-axes align with the build platform, while the Z-axis corresponds to the part's height. The raster angle denotes the direction of deposition relative to the build bed. Layer thickness specifies the thickness of the layer utilized in creating the final part and significantly impacts its properties [62].

The nozzle diameter determines the size of the nozzle, with most commercial printers using a 0.4 mm diameter [63]. When printing short fiber or particle-reinforced composites, larger nozzle sizes are employed to prevent nozzle blockages due to aggregated reinforcements [64]. The number of contours outlines the outer part contours, while raster width indicates the width of the pattern used to fill the parts.

The spacing between neighboring rasters, known as the air gap, is a critical consideration in FDM. Zero air gap printing is strongly recommended since a positive air gap can lead to the separation of rasters [65]. Lastly, infill density defines the percentage of solid material used in constructing the part. For instance, the inner layers of a component might be printed in a hexagonal pattern [18].

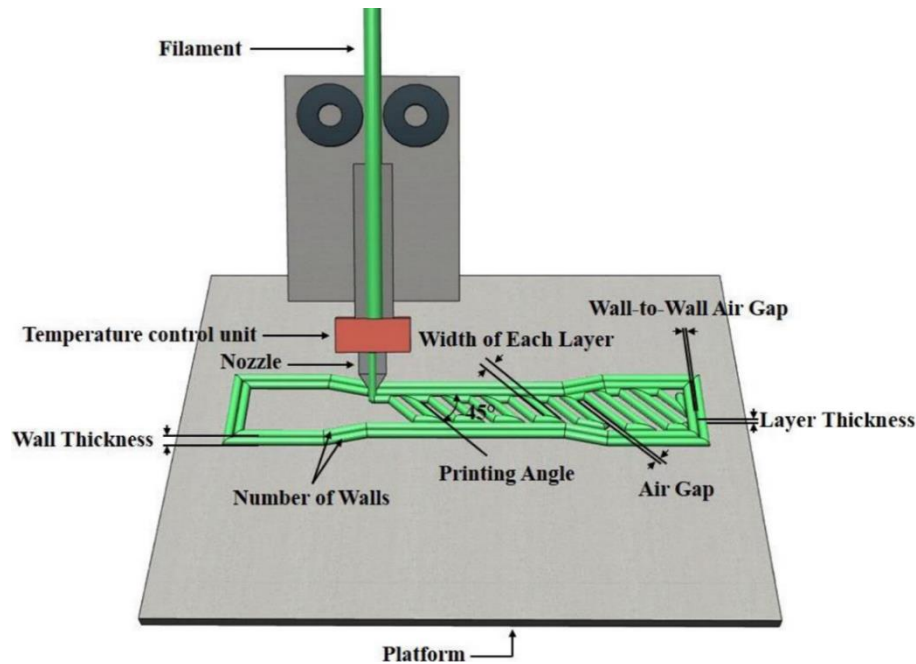


Figure 2.11: FDM process parameters [84]

2.5.3 FDM composites

A composite material or filament typically blends two or more phases or constituents to yield specialized characteristics that a single constituent cannot achieve [85]. In most composites, the matrix and reinforcement represent the primary components, with efforts often directed toward enhancing the matrix's attributes to bolster overall performance.

To improve the overall properties of FDM parts, reinforcement materials such as particulates, fibers, and nanoparticles are added as additional constituents into the polymer matrix (Figure 2.12). The composition, particle size, fiber alignment, and type of reinforcing material all influence the properties of composite materials [17]. While reinforcing materials are often introduced to reduce expenses, they concurrently elevate the functional qualities of FDM constructed components.

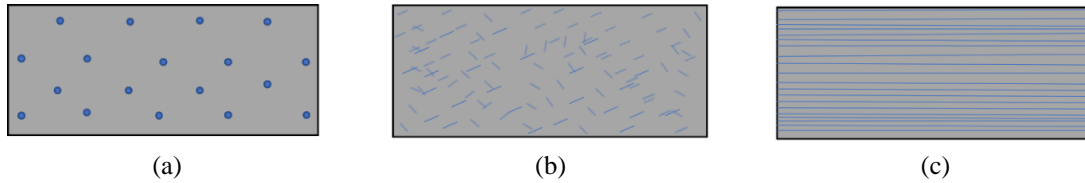


Figure 2.12: In composite filaments, a variety of reinforcing materials are used; (i) Particulate reinforcement (ii) Short fiber reinforcement (iii) Continuous fiber reinforcement

Traditionally, fiber and particulate reinforcements in composites have relied on matrices composed of polymers, metals, or ceramics. In present-day composites, polymers commonly serve as matrix materials and polymer matrix composites possess distinct properties compared to pure polymers [86], making them well suited for the FDM process. The methods used for manufacturing FDM composite filaments and parts are described below. The filler and matrix volume fraction is constrained by the volume fraction of the filler and matrix in the filament. Therefore, any new filler type or volume fraction requires a new filament with the desired volume fractions.

2.5.4 FDM composite preparation methods

FDM composite preparation techniques focus on crafting composite materials tailored for FDM 3D printing. Their primary goal is to improve the mechanical, thermal, or visual qualities of the printed items. The leading approaches for composite preparation are: (a) solution mixing, (b) direct mixing, and (c) in situ.

a. Solution mixing

Solution mixing combines reinforcing elements like carbon fibers, glass fibers, or additives in a solvent to form a consistent solution as shown in Figure 2.13 [87]. This technique enables meticulous management of reinforcing agents within the matrix material, commonly a polymer such as PLA or ABS. Once a uniform solution is attained, the solvent

is evaporated, leaving a composite material. The FDM filament is then obtained from the composite material by extrusion or molding. This method ensures effective dispersion of additives, potentially enhancing the mechanical properties of the final FDM object.

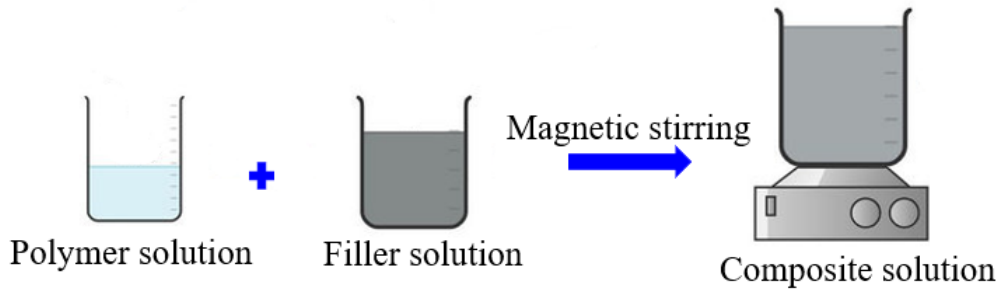


Figure 2.13: Solution mixing [87]

Belaid et al. [19] reported that the addition of GO as a reinforcement to PLA through solution mixing enhanced the tensile strength of FDM PLA parts by 15%. The solution containing GO was introduced into the polymer solution while continuously stirring magnetically until achieving a uniform mixture. This composite polymer solution was then poured into a Teflon dish and left to dry overnight at room temperature. The resulting dried polymer formed a film that was subsequently cut into pieces and fed into a single screw extruder to fabricate filaments suitable for FDM.

b. Direct mixing

In the direct mixing method, the reinforcing agents, like fibers, nanoparticles, or other fillers, are directly and physically combined with the base polymer. This can be achieved through different methods such as melt-compounding or conventional blending techniques (Figure 2.14). Unlike solution mixing, direct mixing does not rely on a solvent and typically demands specialized equipment to guarantee a consistent distribution of additives within

the polymer matrix [88]. While direct mixing can simplify the production of composite filaments, achieving uniform dispersion of fillers can be challenging.

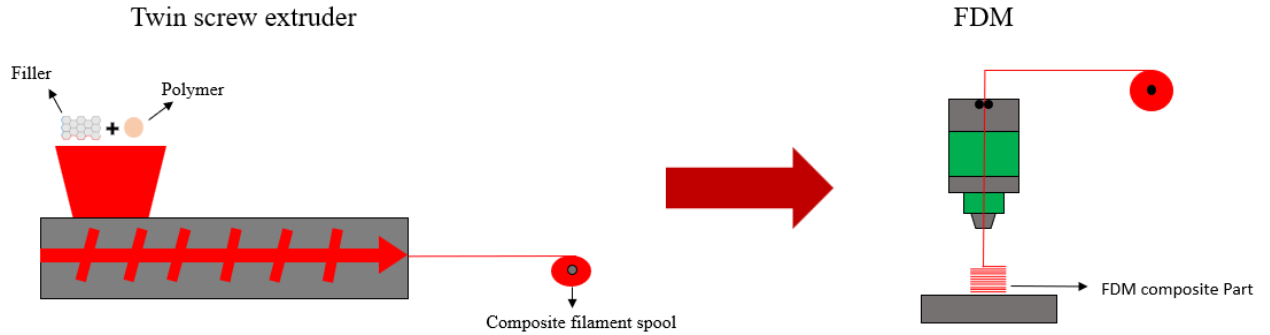


Figure 2.14: Direct mixing via extrusion

Ferreira et al. [88] reported that the addition of carbon fiber as a reinforcement to PLA via direct mixing enhanced the tensile modulus of FDM PLA parts by 113%. Furthermore, Plymill et al. [89] prepared FDM nanocomposites by reinforcing PLA with graphene and multi-walled carbon nano tubes (MWCNT) using a twin-screw extruder. An enhancement in the tensile strength of the printed components was noted with the inclusion of 0.2 wt% graphene and 0.1 wt% MWCNT by 47% and 41% [89].

c. In-situ

In situ FDM printing involves the incorporation of additional reinforcements directly into the printed raster. This includes simultaneously printing and integrating fillers like fibers and particulates. Essentially, it enables the creation of composite structures or functional parts where multiple reinforcements or functionalities are embedded or introduced during the printing process. This technique expands FDM printing capabilities, allowing for the

creation of more intricate, multifunctional, or customized objects in a single manufacturing step as shown below (Figure 2.15).

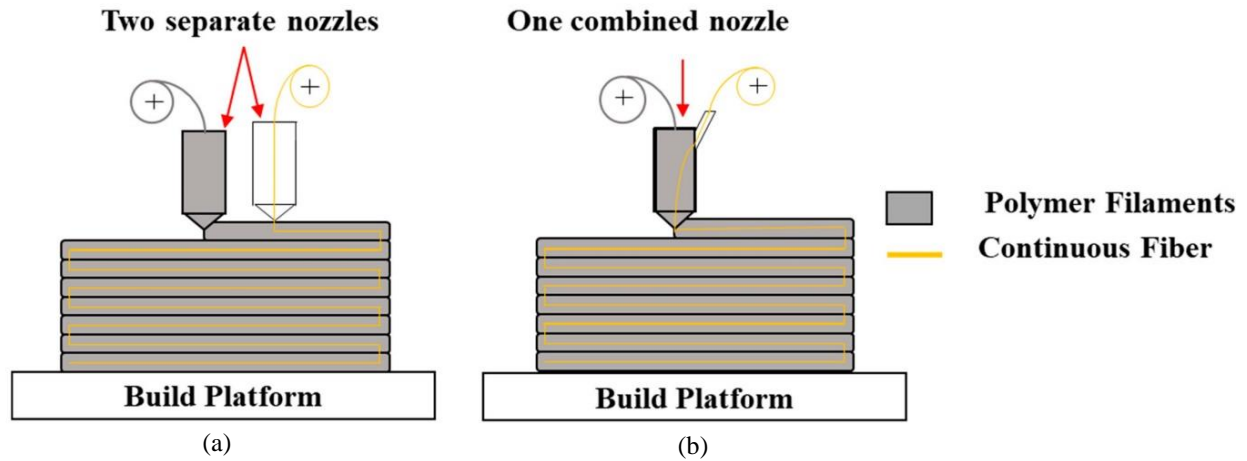


Figure 2.15: FDM in-situ [86]

Some FDM machines are equipped with an additional nozzle to deposit reinforcement materials simultaneously with the polymer layers (Figure 2.15.a). On the other hand, in-situ FDM composites can also be fabricated using one nozzle (Figure 2.15.b). Polymer filament and reinforcement are supplied from two distinct spools that mix in the extruder before being deposited onto the build platform [86]. Li et al. [90] conducted an examination on the effects of continuous carbon fibers on the tensile strength and flexural strength of FDM PLA components. As per their experimental findings, the tensile strength and flexural strength of composite FDM parts exhibited an increase of 185% and 11%, respectively, when compared to parts constructed solely with pure PLA. Hu et al. [91] employed continuous carbon fiber prepreg PLA filament to manufacture composite FDM parts. The FDM machine nozzle was modified to dispense pre-processed continuous carbon fiber prepreg filament. Consequently, the composite parts displayed an increase in both flexural strength and flexural modulus in comparison to the pure FDM PLA parts.

2.5.5 Graphene based FDM studies

Nanocomposites have undergone the least amount of analysis in comparison with particulate, short and continuous fiber-reinforced composites [85]. As this research focuses on GO nanofillers, a broad overview on graphene-based publications is shown in Table 2.3. In all studies, graphene or GO are used as the reinforcements for FDM parts. Graphene is a singular carbon atom thick sheet composed of sp² carbon atoms organized in a honeycomb pattern. Inner and outer plane bonds connect two corresponding sub-lattices of carbon atoms, forming a delocalized network of electrons [92]. These distinct properties are why graphene was chosen as a reinforcement for polymeric matrices in FDM. In graphene based FDM composites, the adhesion between the graphene nanoparticles and polymeric matrices is crucial in order to achieve better parts with superior properties [93].

Belaid et al. [19] reinforced PLA by incorporating graphene oxide as a nanofiller via solution mixing to manufacture FDM PLA-GO scaffolds and investigate their mechanical, thermal, and morphological properties. Overall, the results depicted that the integration of GO resulted in rougher surfaces and enhanced hydrophilicity, unchanged transition temperature, reduced polymer crystallinity, and improved scaffold mechanical properties.

Zhang et al. [20] created FDM PLA-GO flexible circuits via melt blending by utilizing graphene and employing a two-step in-situ tailored reduction technique for synthesizing reduced GO. The printed parts were mechanically and morphologically characterized to analyze the FDM PLA-GO parts. Their findings suggested that the FDM PLA-GO parts exhibited smooth surfaces with tremendous mechanical properties.

Table 2.3: Publications on FDM PLA-graphene

Reference	Matrix	Nanocomposite Material	Filler %	Printer
Belaid et al. [19]	PLA	Graphene oxide	0.2%	Prusa i3 MK2S
Zhang et al. [20]	PLA	Graphene oxide	4-6%	MakerBot Replicator2
Wei et al. [21]	ABS, PLA	Graphene Oxide	0.4-7.4%	HOF1-X1
Chen et al. [22]	TPU+PLA	Graphene Oxide	0-5%	-
Wu et al.[23]	PLA	Graphene Oxide	0-9%	AllcctTank dual-nozzle
N. Vidakis et al. [94]	PLA	Graphene	-	da Vinci 3-in-1 Pro
Bustillos et al. [95]	PLA	Graphene	-	MakerBot Replicator
Prashantha and Roger [96]	PLA	Graphene	10%	-
Javaid et al. [97]	PLA	Graphene	-	Anet ET4 Pro
Shi et al. [98]	PLA	Graphene	0.5-10%	RepRap X350pro
Camargo et al. [99]	PLA	Graphene	-	Delta_3D
Daniel et al. [100]	PLA	Graphene	5.6%	MakerGear M2
Ivanov et al. [101]	PLA	Graphene	0-6%	-
Novotny et al. [102]	PLA	Graphene	-	Prusa i3 MK3
Spinelli et al. [103]	PLA	Graphene	3-6%	Rep Rap X400 Pro
Flavio et al. [104]	PLA	Graphene	0.5-5%	Ultimaker S3
Plymill et al. [89]	PLA	Graphene	0.1-0.5%	LulzBot Mini printer
Camintero et al. [105]	PLA	Graphene	-	BQ WitBox
Batakliiev et al. [106]	PLA	Graphene	1.5-12%	RepRap X400 pro
Rostom and Dadmun [107]	PLA	Graphene	0.5-2%	LulzBot TAZ5

Chen et al. [22] showcased the FDM fabrication of PLA/TPU-GO composites and evaluated their suitability in terms of biocompatibility. The FDM composites were developed using a solvent mixing technique. The addition of GO significantly improved the mechanical characteristics and thermal stability of the composites.

Vidakis et al. [94] experimentally determined the mechanical response of FDM specimens produced using PLA and PLA-graphene. The PLA-graphene FDM parts were printed using a commercially available PLA-graphene filament. Various standard mechanical tests were conducted to assess their mechanical properties and enable a comparison between the two materials. Ultimately, the results showed that, under identical printing parameters, the FDM PLA parts exhibited superior stiffness, and a greater extent of brittleness compared to the FDM-graphene parts.

Bustillos et al. [95] compared the characteristics of FDM parts made from PLA-graphene filaments to those of pure PLA parts. According to their experimental investigation, all mechanical properties (creep resistance, elastic modulus, wear resistance and nano hardness) showed improvement. Moreover, because of the weak interlayer bonding, PLA-graphene architectures showed significant levels of porosity when compared to pure PLA components

Camargo et al. [99] evaluated the mechanical properties of 3D printed FDM PLA-graphene components that were printed using a commercially available PLA-graphene filament. Using a statistical central composite design approach, they investigated variations in infill density and layer thickness. Their research demonstrated that increasing layer thickness improved mechanical characteristics.

Flavio et al. [104] assessed the impact of graphene on the tensile and compressive properties of FDM PLA parts. The PLA-graphene parts were printed with PLA-graphene filaments. The tensile and compressive properties of their FDM PLA-graphene parts were

superior to the pure FDM PLA parts. Furthermore, the mechanical properties of the FDM PLA-graphene parts were improved by increasing the graphene weight percentage.

Plymill et al. [89] conducted tensile and impact study to evaluate the mechanical properties of FDM PLA-graphene parts manufactured by the means of dry mixing followed by twin-screw extrusion. DSC was used to examine the thermal parameters of the feedstock material and printed parts. The inclusion of graphene improved mechanical characteristics of FDM PLA parts. Prashantha et al. [96] investigated the tensile properties of FDM PLA-graphene parts using a commercially available 10% PLA-graphene filament. In comparison to pure PLA parts, nanocomposite parts showed increased tensile modulus, TS, with lower ductility.

The results from literature highlight the importance of GO in improving the FDM part properties with various materials. In this work, FDM PLA-GO parts were studied using a novel in-situ nozzle impregnation technique. The PLA and PLA-GO part properties under various loading conditions are described and compared to these experimental works in Chapter 4.

CHAPTER 3

EXPERIMENTAL METHODOLOGY

This chapter entails a detailed discussion on the novel in-situ nozzle impregnation technique that was implemented in this work to fabricate the FDM PLA-GO parts. In addition, details about the various characterization and testing techniques are presented. It should be noted that all tests were conducted on three repetitions to guarantee repeatability of experimental data.

Commercial polylactic acid (PLA) filament was used as a matrix and Graphene oxide (GO) 1% dispersion acquired from GOgraphene® was used as a reinforcement. In this work, 3D printing was carried out on a Creality Ender 3 pro with a filament size of 1.75 mm, nozzle size of 0.4 mm, extrusion speed of 30 mm/s, nozzle temperature of 230°C and a build plate temperature of 70°C. All parts were printed with an infill of 100% using variable layer thicknesses (0.15 mm and 0.3 mm). To fabricate PLA-GO 3D printed composite parts, the GO solution was loaded in a 5mL syringe and held inside an automatic syringe pump at a control rate of feed of 0.5mL/hr. This control rate helped maintain the back pressure in the print head. The GO solution was injected into the hot end through secondary tubing as shown in Figure 3.1. The mixing of GO and PLA was achieved in a custom designed hot end assembly. Upon reaching the heating block, the GO solution evaporated leaving a mixture of PLA and GO (Figure 3.1). This mixture was further mixed inside the nozzle before being deposited on the build plate to produce FDM-GO parts. Table 3.1 summarizes

the FDM process parameters used to print the pure PLA and graphene oxide infused PLA parts.

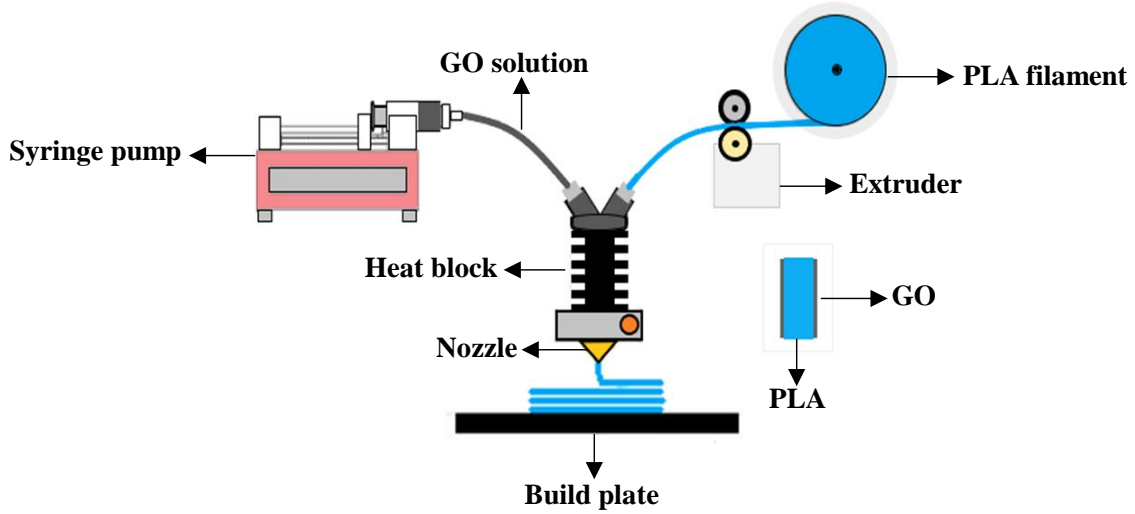


Figure 3.1: FDM nanocomposite preparation method

Table 3.1: Selected FDM process parameters

Parameter	Specification
Material	PLA & PLA-GO
Nozzle diameter	0.4mm
Nozzle temperature	230°C
Print bed temperature	70°C
Filament diameter	1.75mm
Layer thickness	0.15, 0.3 mm
Infill density	100%
Nozzle speed	30 mm/s
Raster angle	45°

Characterization of the PLA and PLA-GO samples was conducted on various sample types as discussed below. In addition, PLA and PLA-GO samples with varying layer heights

were manufactured to test the tensile, compressive, flexural and impact properties. Detailed dimensions are given in Figure 3.2.

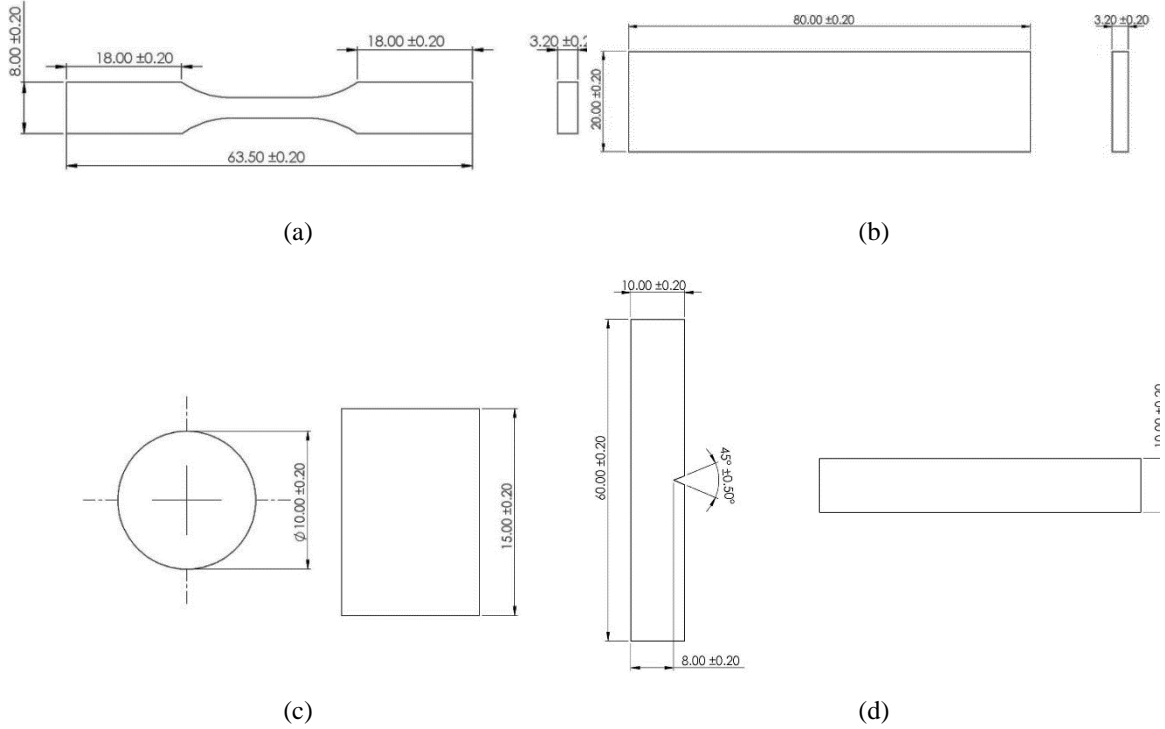


Figure 3.2 Dimensions of PLA and PLA-GO samples for; (a) Tensile tests, (b) Flexural tests (c) Compression tests, (d) Impact tests

3.1 Scanning electron microscopy (SEM)

SEMoscope IEM11+ (Figure 3.3) was used at 20 kV under vacuum for the characterization of printed samples. All samples were sputter coated pre analysis for 30s and the as-printed, and fracture surfaces from tensile samples were analyzed.

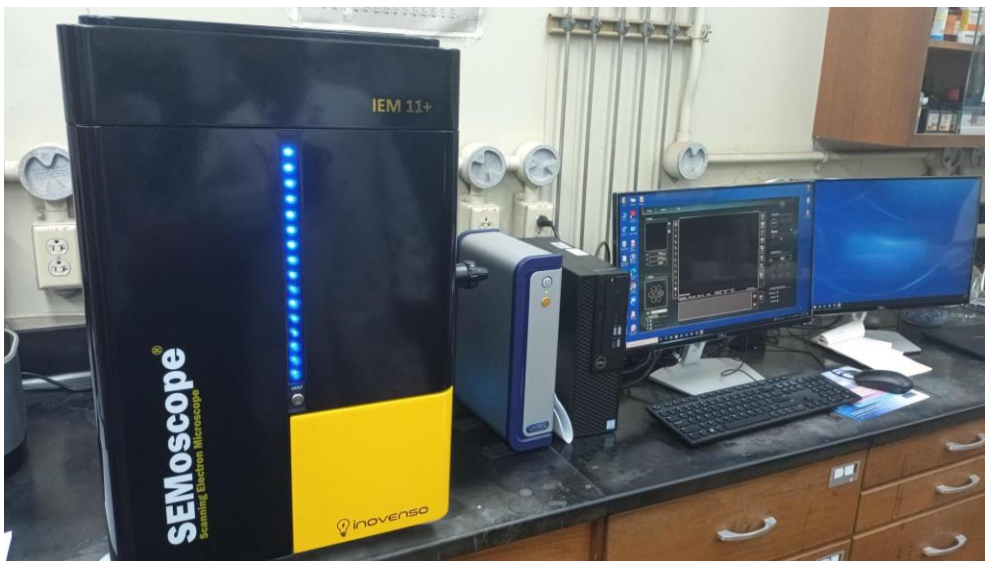


Figure 3.3: SEMoscope IEM11+

3.2 Thermogravimetric analysis (TGA)

TGA was carried out using a SDT Q600, TA Instruments machine (Figure 3.4) to evaluate thermal stability of PLA and PLA/graphene samples. Samples were heated from 25°C to 600°C, under a 50 mL/min flow of nitrogen at heating rate of 10°C/min. TRIOS software (TA Instruments) was used to analyze the data.

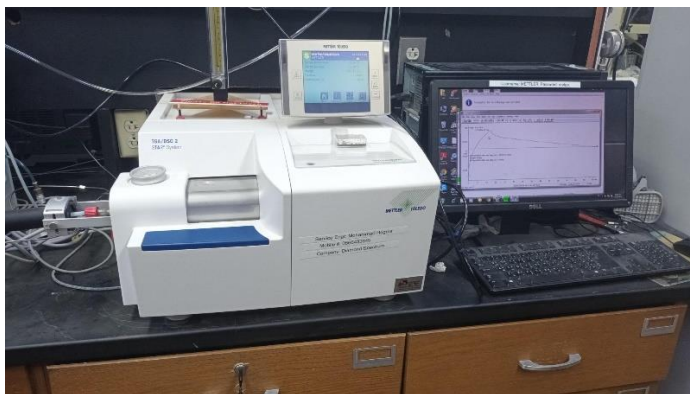


Figure 3.4: TA Instruments SDT Q600 TGA machine

3.3 Differential scanning calorimetry (DSC)

DSC employing a heat/cool/heat regimen (DSC Q2000, TA Instruments) was employed to assess thermal characteristics (Figure 3.5). The samples underwent heating at a rate of 10°C per minute up to 220°C and subsequent cooling at the same rate to 30°C, all conducted under a nitrogen atmosphere at a flow rate of 50 ml/min. Analysis of the data was performed using TRIOS software (TA Instruments). The calculation of crystallinity (X_c) for the PLA polymer was found using the equation below.

$$X_c = (\Delta H_m / \Delta H_m^o) \times 100 \quad (1)$$

where ΔH_m^o is the melting enthalpy of 100% crystalline PLA ($\Delta H_m^o = 93 \text{ J/g}$), is the crystallinity% and ΔH_m is the recorded melting enthalpy for the FDM parts.



Figure 3.5: (DSC) Q2000 V24.9 TA instruments® machine

3.4 X-ray diffraction (XRD)

The FDM PLA-GO parts crystallinity and phases were identified using Rigaku Mini Flex II XRD machine (Figure 3.6). The peaks and diffraction angles for both FDM PLA and FDM PLA-GO were obtained between 0° to 100° with a step size of 0.02°.



Figure 3.6: Rigaku® Mini Flex II XRD machine

3.5 Fourier transform infrared spectroscopy (FTIR)

FTIR was performed on the samples using Thermo scientific Nicolet iS10 spectrometer (Figure 3.7) equipped with ATR technique. The Measurements were taken in the range of wave numbers of 400 to 4000 cm^{-1} .



Figure 3.7: Nicolet iS10 FTIR machine

3.6 Tensile, compressive, and flexural test

The tensile tests specimens were prepared according to the ASTM D638 standard consisting of different compositions and layer heights. Tensile tests were conducted using a Instron® 3367 Universal Testing System as shown in Figure 3.8.a with a load cell of 30 kN and a cross-head velocity of 2 mm/min. The analysis of the experimental data provided essential mechanical properties, including TS, tensile strain, and tensile modulus, for both FDM PLA and FDM PLA-GO specimens. Furthermore, a 12 mm extensometer was also equipped for this test to precisely measures changes in length as the material stretches or deforms. An Instron®, catalogue 2620-601 12 mm extensometer with the range of ± 5 mm was also used to record the strain in the gauge section of the tensile tests.

The compression test samples were prepared following the ASTM D695 standard and were tested on an Instron 5569® Universal Test System (Figure 3.8.b) was utilized with a load cell of 50kN at a cross-head velocity of 2 mm/min. Following the standard's requirements, the compressive strength, and the compressive modulus of the tested specimens were recorded.

Flexural tests were performed according to ASTM D790 (three-point bending of polymers) All flexural tests were carried out on an Instron® 3367 Universal Test System at a cross-head velocity of 2 mm/min (Figure 3.8.c). Bending characteristics such as flexural strength, flexural modulus, and displacement were obtained from these tests.

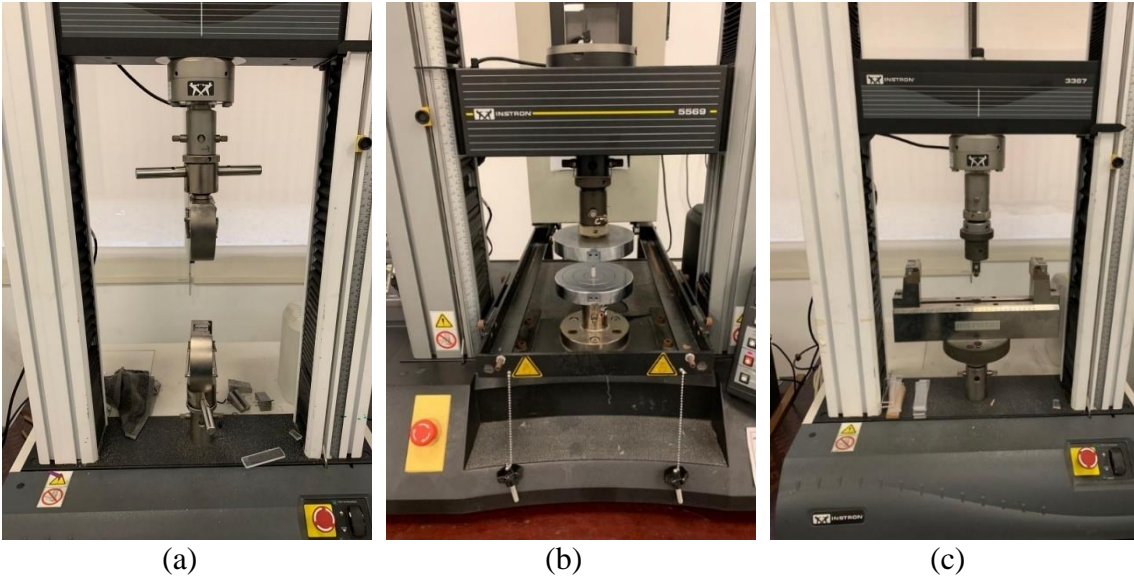


Figure 3.8: (a) Instron® 3367 Universal Test System tensile test setup (b) Instron® 5569 Universal Test System compression test setup (c) Instron® 3367 Universal Test System flexural test setup

3.7 Impact test

In accordance with ASTM D6110 guidelines, FDM specimens were created for impact testing using a 25 Nm gunt® WP 400 impact testing machine (Figure 3.9). The test was conducted to determine the impact energy (J) of both FDM PLA and FDM PLA-GO samples.



Figure 3.9: gunt® WP 400 Impact test machine

3.8 Hardness and micro-hardness

The Rockwell-R testing scale was used for macro-hardness measurements and were carried out using a Rockwell apparatus by Tinius Olsen (Figure 3.10.a) with a load of 60kgf. Additionally, the Vickers test was used to find the microhardness of the FDM samples. A Nextgen NG-1000CCD machine (Figure 3.10.b) was selected for this test using a 0.1 kg load with a 15 s indentation duration. The specimens' polished surfaces were pressed with a conventional Vickers diamond pyramid indenter.



(a)



(b)

Figure 3.10: (a) Tinius Olsen hardness test machine (b) Nextgen Micro Vickers hardness machine

CHAPTER 4

RESULTS AND DISCUSSION

This chapter delves into an in-depth examination of the findings stemming from an array of mechanical, thermal, and morphological evaluations conducted on FDM-produced PLA and PLA-GO components. The exploration of these outcomes serves as a critical investigation, providing insights on the impact of integrating GO and the change in layer height on the mechanical attributes, thermal properties, and surface characteristics of FDM PLA parts, offering a deeper comprehension of their potential applications and performance across diverse scenarios.

4.1 Scanning electron microscope (SEM)

SEM is an excellent tool for determining the purity, level of aggregation, dispersion, and homogeneity of the GO nanoparticles in the FDM PLA-GO parts [108]. An example of the printed PLA and PLA-GO parts is shown in Figure 4.1.a. Printed PLA-GO clearly show the presence of GO in the PLA matrix. SEM images from the PLA and PLA-GO samples are also shown in Figure 4.1b-c. Compared to the PLA samples; the PLA-GO clearly show a lack of surface cracks. This might have an effect on the mechanical properties of these parts as presence of cracks may facilitate early fracture resulting in low ductility and strength.

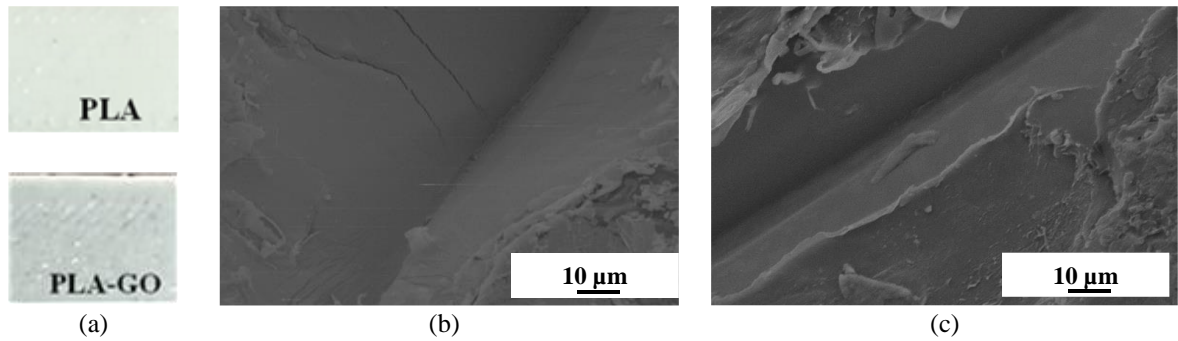


Figure 4.1: (a) PLA and PLA-GO samples SEM images of (b) PLA, (c) PLA-GO

Furthermore, the SEM images below (Figure 4.2) verify the existence of GO nanoparticles embedded in the PLA matrix. Figure 4.2 shows the presence of GO nanoparticles embedded between the FDM PLA layers while the inset shows a GO particle within the PLA matrix.

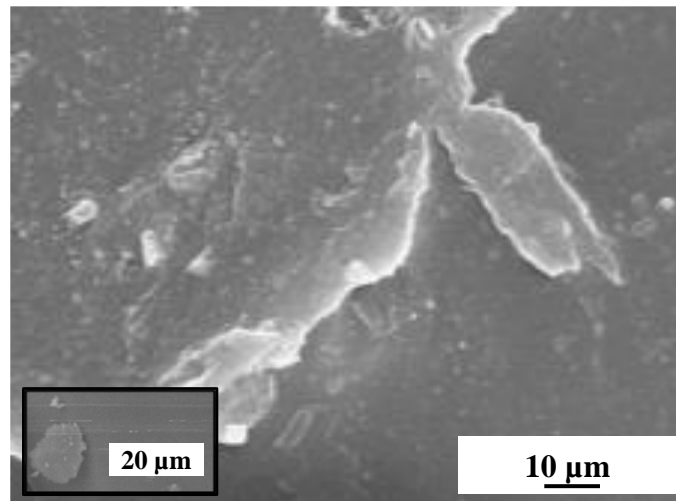


Figure 4.2: FDM PLA-GO SEM images

4.2 Thermogravimetric analysis (TGA)

TGA stands as a potent method for assessing the thermal stability of various materials, including polymers [109]. This technique involves monitoring changes in a specimen's weight as its temperature is incrementally raised. TGA is capable of measuring both

moisture and volatile contents within a sample. The apparatus comprises a highly sensitive scale to track weight variations and a programmable furnace to regulate the sample's heat levels. The thermal stability of FDM PLA and PLA-GO were analyzed using TGA to examine the influence of the GO nanofiller on the PLA matrix and assess the percentage of GO in PLA-GO samples (Figure 4.3). A 5 wt% loss was recorded at 306°C for the FDM PLA sample, while the FDM PLA-GO samples measured a 5 wt% loss at 317°C. Furthermore, the temperatures at which the FDM samples recorded a 50 wt% loss (Maximum degradation temperature peak) were also measured. According to the results summarized in Figure 4.3, the FDM PLA samples recorded a 50 wt% at 357°C and the FMD PLA-GO samples recorded the same wt% at 362°C. This is important as it indicates the presence of graphene oxide in the PLA matrix because the T50 increased with the addition of GO. Therefore, the addition of GO increased the maximum thermal degradation temperature as shown in Figure 4.3. The interfacial interactions between GO and PLA caused by hydrogen bonds and/or van der Waals forces may account for this shift [110], [111]. In addition, the residual wt% was measured to account for the addition of graphene. The FDM PLA samples recorded a residual wt% of 1.32, while the FDM PLA-GO showed an increase with a measured value of 2.32% (Table 4.1). Therefore, the PLA-GO samples are assumed to have an average 1 wt% GO.

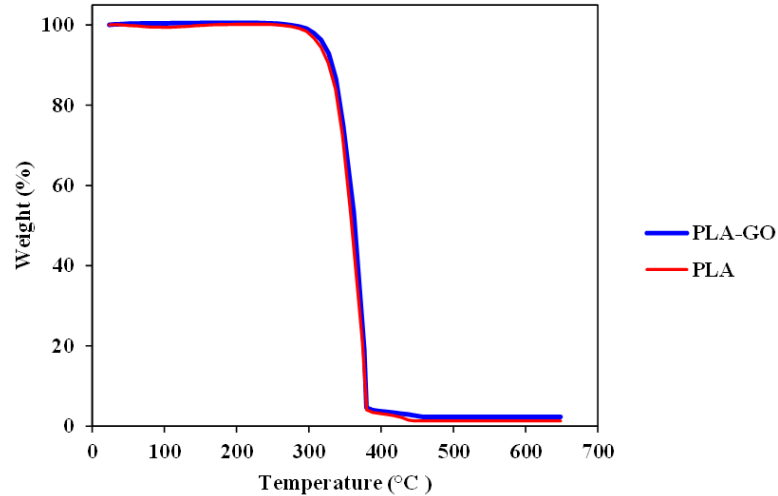


Figure 4.3: TGA curves for FDM PLA and PLA-GO

Belaid et al. [19] carried out TGA tests on FDM PLA and PLA-GO samples to investigate the addition of graphene oxide as a nanofiller. According to the study, the adsorbed water was the cause of the 1% weight loss for PLA that was observed below 200°C. Between 300 and 400°C, the second significant weight loss was due to the polymer’s degradation. The derivative weight curves indicated that in the nanocomposites containing 0.3% GO, the highest degradation temperature peak shifted from 298°C to 366°C [19]. In their work, the thermal stability of FDM PLA-GO parts improved as a result of the strong interactions with GO, as a result of a reduction in chain mobility at the GO interface [112]. When reinforced with GO, the PLA-GO pyrolysis of labile oxygenation groups causes the thermochemical breakdown of the remaining organic content from PLA and GO [113], which was the cause of the final weight loss from 400 °C [19].

Table 4.1: TGA results for PLA and PLA-GO

Sample	T5 (°C)	T50 (°C)	Residual wt (%)	DTG Peak (°C)
PLA	306	357	1.31	357
PLA-GO	317	362	2.32	362

On the other hand, Chen et al. [22] reported different findings as their FDM PLA/TPU parts had a better thermal resistance compared to the FDM PLA-GO/TPU-GO parts. It has been reported that at the highest temperature the FDM PLA/TPU-GO sample measured a greater weight loss percentage than that of pure PLA/TPU sample. This difference could be attributed to the use of copolymer as a matrix (PLA/TPU) instead of PLA.

4.3 Differential scanning calorimetry (DSC)

The DSC technique holds immense significance in polymer analysis due to its ability to offer critical insights into their thermal properties [114]. It identifies melting and crystallization temperatures, delineating transitions from solid to liquid states. Additionally, DSC determines the Glass Transition Temperature (T_g), indicating when polymers shift from a rigid to a flexible state as well as the degree of crystallinity (X_c %) in semi-crystalline polymers, making it possible to evaluate their mechanical characteristics and structural arrangement. Figure 4.4 shows the DSC spectra of both PLA and PLA-GO samples to analyze the effect of GO on the PLA matrix. According to the results summarized in Figure 4.4, the T_g was slightly decreased with the addition of graphene oxide from 59.3 to 59°C, while the T_m remained unaltered at 148.9°C. Furthermore, the X_c % reduced with the incorporation of GO from 35.8 to 27.6 %. Other studies have also concluded that the addition of graphene oxide and graphene had a negative impact on the T_g and X_c % of FDM PLA parts [19], [95]. This was attributed to the swift cooling observed in FDM PLA-GO parts during the FDM process, which limits its fluidity and mobility and prevents polymer chains from rearranging themselves resulting in the reduction of crystalline regions in the FDM nanocomposite [115]. The PLA part measured a X_c of 34%, meanwhile the FDM PLA-graphene recorded a X_c of 31% [95].

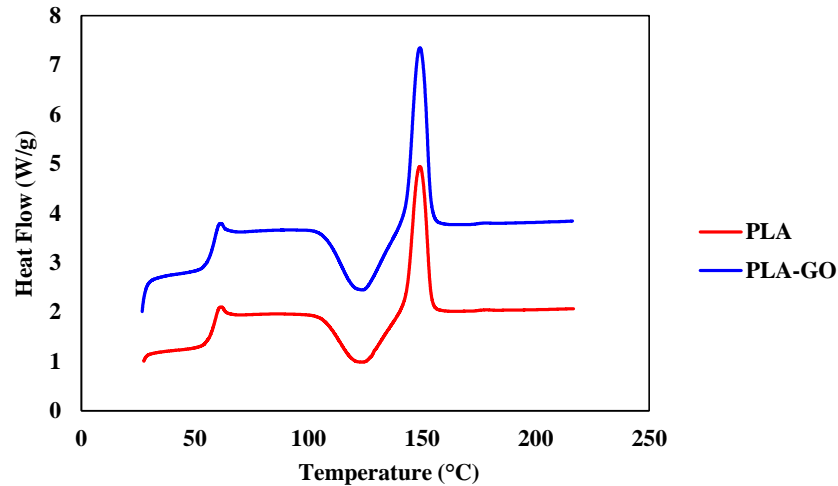


Figure 4.4: PLA and PLA-GO DSC curves

On the other hand, GO has also been reported to increase the $X_c\%$ of FDM PLA-GO parts as a higher number of interactions are expected between the polymer chains with the incorporation of the functionalized nanofiller [19]. The following study investigated the effect of different graphene oxide (GO) wt% on the $X_c\%$ of FDM PLA parts [19]. The FDM PLA-GO sample with a 0.1% GO wt% recorded the lowest X_c (0%), while the FDM PLA-GO part with a 0.3% GO wt% achieved the highest X_c (45%) [19]. The reported increase was attributed to the increase in the crystalline regions of the FDM PLA part with the addition of GO (Figure 4.5). The presence of GO in the FDM PLA parts can lead to an increase in its molecular weight, which can result in an increase of the Vander Waal forces. These intermolecular forces can contribute to the stabilization and organization of the crystalline regions [116]. Hence, an increase in crystallinity (X_c) can bolster a material's capacity to endure external forces without experiencing undue distortion or structural breakdown [117].

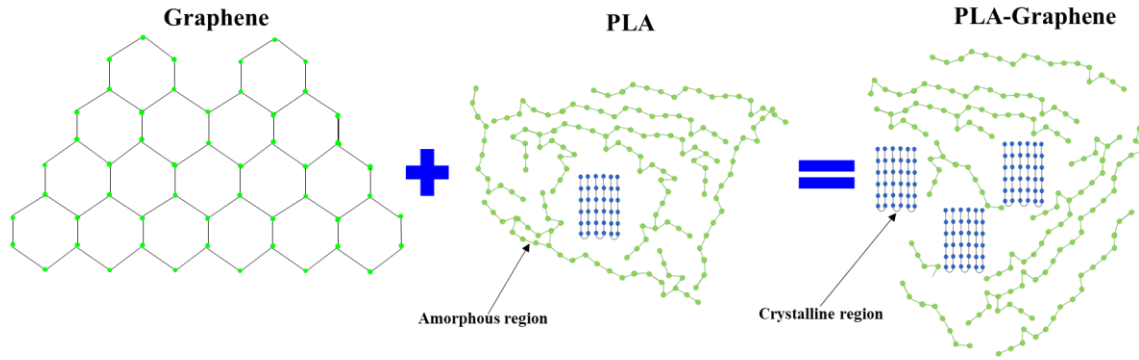


Figure 4.5: The effect of graphene on the crystallinity of PLA

Moreover, the melting enthalpy (ΔH_m) has been reported to diminish with the introduction of GO. The FDM PLA parts recorded a ΔH_m of 33.6 J/g, while the FDM PLA-GO parts achieved a ΔH_m of 25.9 J/g (Table 4.2). The result is in-line with other observations as the ΔH_m was expected to decrease with the addition of GO due to the reduction in crystallinity. The energy required to melt the material (ΔH_m) is directly proportional to the crystallinity of the FDM parts, hence a lower ΔH_m was recorded by the FDM PLA-GO parts since its $X_c\%$ decreased [118]. Results in literature have also reported that the FDM PLA-GO parts with a 0.2 and 0.3% GO wt% recorded higher ΔH_m values (43 and 40 J/g) compared to the parts with the 0.1% loading (27 J/g) [19].

Table 4.2: FDM PLA and PLA-GO DSC results

Sample	Tg (°C)	Tm (°C)	Xc (%)	DHm (°C)
PLA	59.3	148.8	35.8	33.6
PLA-GO	59	148.9	27.6	25.9

4.4 X-ray diffraction (XRD)

XRD offers insights into the structure and properties of materials. It aids in assessing crystallinity, identifying structural phases, and characterizing materials such as complex polymer blends or composites [119]. According to the results (Figure 4.6), the FDM PLA parts showed two characteristic peaks at the diffraction angles 20 and 27.5°, while the FDM PLA-GO parts recorded two characteristic peaks at 18 and 27°. The peaks were observed at similar diffraction angles, however the FDM PLA-GO peak shown at 18° was much broader compared to the first peak shown by the FDM PLA parts at 20°. This change is attributed to the interactions between GO and PLA, which has the potential to disturb PLA's crystalline arrangement. This disturbance occurred as the GO particles impeded the creation of clearly defined crystalline regions within the PLA matrix, resulting in a wider characteristic peak as shown in Figure 4.6. This explanation was backed by the fact that the crystallinity % of the FDM PLA parts decreased with the addition of GO.

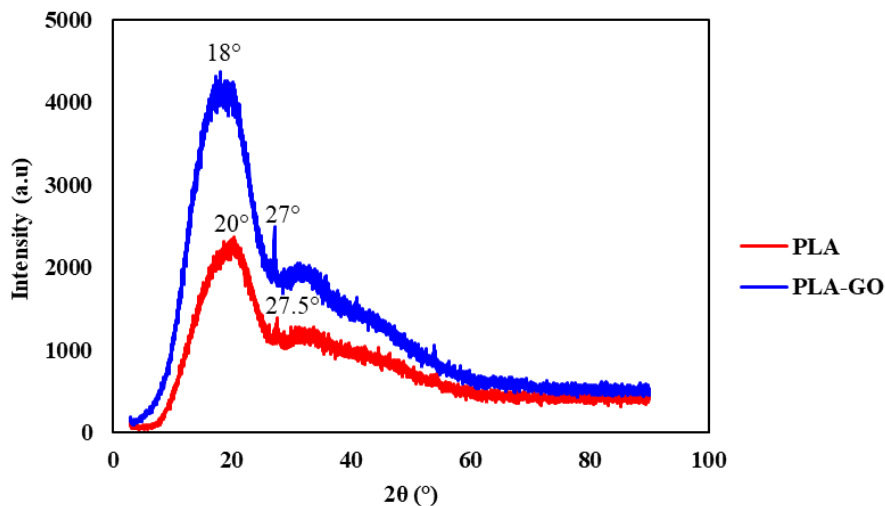


Figure 4.6: PLA and PLA-GO XRD results

The literature reports that the PLA filament revealed four distinct peaks at $2\theta = 15, 17, 19,$ and 23° that indicated the α form of PLA [19], [120]. The alpha form of PLA signifies a particular crystalline arrangement within its structure that affects the PLA's properties, including mechanical strength and thermal behavior, by organizing its molecular chains in a specific lattice structure [121]. Furthermore, the PLA crystalline peaks vanished after being subjected to the FDM process [19]. The disappearance of the crystalline peaks in PLA after filament extrusion might be attributed to the rapid cooling process during FDM. When PLA melts during printing and encounters quick cooling, often in an open environment, it prevents the rearrangement of its crystalline structure, leading to the absence of distinct crystalline peaks in the material analysis.

The addition of GO to the FDM PLA parts was also investigated [19]. Before extrusion, the PLA-GO parts displayed broader PLA characteristic peaks at $2\theta = 17$ and 23° compared to PLA filament due to micro-stresses caused by the addition of GO. The absence of a distinctive GO peak could be due to low filler concentration or effective GO dispersion [19], [120]. Post-extrusion, a similar pattern was observed with two broad peaks shown between 10 and 25° in the FDM PLA-GO part, indicating an amorphous nature of the polymer [19].

4.5 Fourier transform infrared spectroscopy (FTIR)

In polymer nanocomposites, enhancing mechanical properties usually depends on ensuring an even dispersal of the filler within the matrix, a distribution which is impacted by relations between the filler and the matrix [22].

FTIR is an analytical technique which plays a crucial role in polymer analysis by identifying the functional groups within polymer molecules, enabling a detailed examination of their chemical structure and composition [122]. FTIR was conducted to analyze the interaction between the PLA matrix and GO by investigating their distinct functional group vibrations when exposed to particular light wavelengths. This helps in understanding the complex molecular arrangements and chemical properties of polymers, aiding in their comprehensive characterization and application in diverse industries.

As depicted in Figure 4.7, the FDM PLA component displays distinct peaks at 1037, 1080, and 1180 cm^{-1} , corresponding to C-O-C stretching vibrations [123]. Additionally, a peak is evident at 1746 cm^{-1} , associated with the C=O stretching vibration [124], along with three other peaks at 2833, 2903, and 2974 cm^{-1} , related to the uneven and even stretching vibrations of the CH₃ group [123]. Figure 4.7 also shows that the GO characteristic peaks were recorded at 3434, 2362 and 1627 cm^{-1} . These distinctive peaks signify specific functional groups existing within the FDM PLA-GO parts. The 3434 cm^{-1} peak typically signifies O-H stretching vibrations, indicating the existence of hydroxyl groups in GO [125]. At 2362 cm^{-1} , the peak corresponds to C=O stretching vibrations, representing carbonyl groups (C=O) inherent in the GO structure [126]. Additionally, the 1627 cm^{-1} peak commonly denotes C=C stretching vibrations, implying the existence of aromatic rings or double bonds within the GO structure [127].

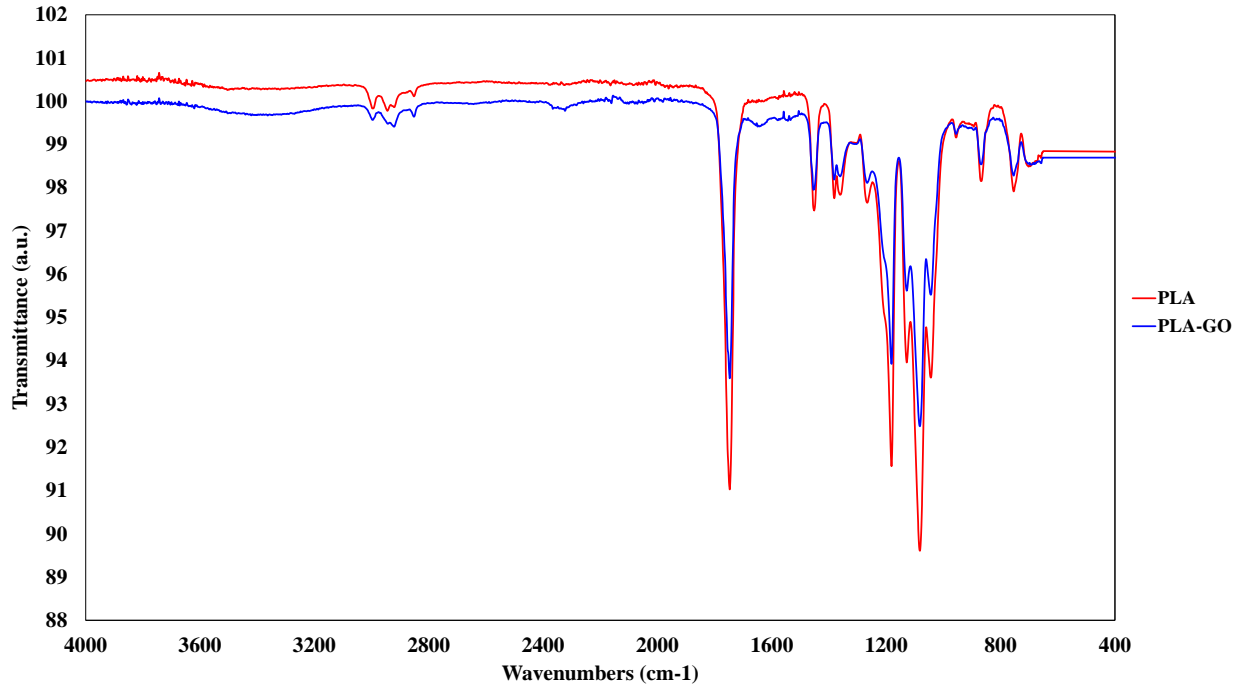


Figure 4.7: FTIR results for FDM PLA and PLA-GO

Belaid et al. [19] noted that GO's distinct features were identified via bands observed at specific frequencies: 1040 cm^{-1} (C-O elongation vibrations) and 1740 cm^{-1} (C=O elongation vibrations of the carbonyl and carboxylic groups). Furthermore, at 1630 cm^{-1} another peak is observed likely denoting the skeletal vibration of graphite domains, while a broader range between $3000\text{--}3500\text{ cm}^{-1}$ was associated with hydroxyl groups [19], [22]. Despite this, there was no observable difference between the peaks of pure FDM PLA and FDM PLA-GO components. The stronger absorption of the PLA peak, which fell within a similar range to GO, posed a challenge in identifying specific GO peaks within the FDM PLA-GO nanocomposite [19].

4.6 Tensile test

Tensile tests reveal essential characteristics such as TS, tensile modulus, and ductility for a plethora of materials [128]. The graphical representation of the tensile stress-strain

outcomes for the FDM specimens utilized in this research are presented in Figure 4.8.a. These findings highlight the effect of the layer height on the TS of both PLA and PLA-GO samples.

The data indicates that varying the layer height affects the TS of Pure PLA FDM samples. For instance, the average TS was measured at 42.5 MPa for the Pure FDM PLA 0.15LH samples, while the Pure FDM PLA 0.3LH samples exhibited an average TS of 43.5 MPa (Figure 4.8.b). However, according to previous studies, there is a tendency for the TS of FDM PLA samples to decrease as the layer height is increased [129], [130]. A larger layer height reduces the cooling/heating cycles and leads to fewer sliced layers. Therefore, the chance of deformation, delamination, and failure in the produced parts during FDM processing hence increases [130].

Moreover, a similar trend was observed in the FDM PLA-GO samples, where those with greater layer heights exhibited higher tensile strengths. Specifically, the PLA-GO 0.15LH samples demonstrated an average TS of 48.5 MPa, while the PLA-GO 0.3LH samples showcased an average TS of 50 MPa. These findings, depicted in Figure 4.8.b, highlight the effect of GO on the TS of both the pure PLA 0.3LH and PLA 0.15LH FDM samples. This improvement is attributed to robust intermolecular connections between the nanofiller and the polymeric matrix [131], primarily driven by Vander Waals and hydrogen bond interactions [132]–[134]. Additionally, the results highlight that the increase in layer thickness elevated the TS of PLA samples by 2.4% and PLA-GO samples by 3.1% due to adequate bonding between the layers.

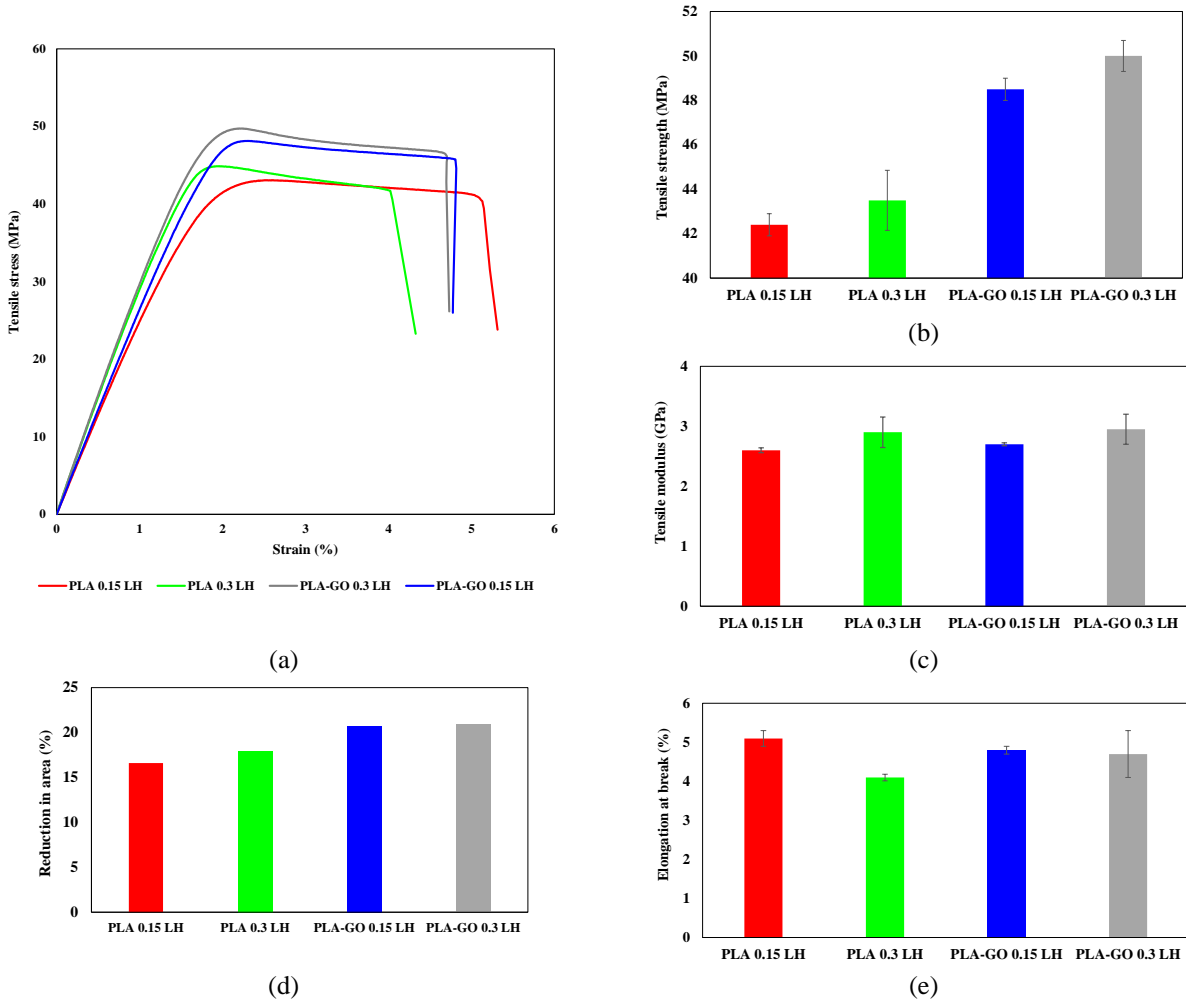


Figure 4.8: (a) Tensile- stress vs strain curves, (b) Tensile strength (TS) (c) Tensile modulus, (d) Reduction in area (e) Elongation at break

Moreover, the height of the layers significantly impacts the tensile modulus of FDM samples. As shown in Figure 4.8.c, the FDM PLA 0.15LH samples demonstrated an average tensile modulus of 2.6 GPa, whereas the FDM PLA 0.3LH samples exhibited a higher average of 2.9 GPa. Adding graphene as a filler increased the tensile modulus of the FDM PLA 0.3LH samples from 2.90 to 2.95 GPa (1.7%). Similarly, the FDM PLA 0.15LH samples experienced a slight rise from 2.6 to 2.7 GPa (3.8%). This change in tensile modulus for both PLA and PLA-GO samples highlights graphene's capacity to fortify and improve resistance to elastic deformation when subjected to tensile loads. Therefore, the

addition of GO has a higher significance on the tensile properties of FDM PLA parts compared to the change in layer height.

The elongation at break, denotes the percentage increase in length of a material sample before it fractures during tensile testing [135]. The elongation at break (%) observed in Figure 4.8.e showed a slight reduction in FDM PLA 0.15LH, reducing from 5.1% to 4.8% when graphene was added, likely due to potential voids forming between deposited layers [96]. Conversely, the presence of graphene in the FDM PLA 0.3LH samples increased the elongation at break (%) from 4.1% to 4.7%. This variation could be linked to the specific arrangement and controlled distribution of graphene filler within the PLA 0.3LH matrix. Higher elongation at break % indicates greater ductility, allowing more plastic deformation before failure.

Similarly, the reduction in area % was computed as a measure of ductility exhibited by the FDM samples [136]. As illustrated in Figure 4.8.d, FDM PLA 0.15LH parts experienced a 16.6% reduction in area, while the FDM PLA 0.3LH parts showed an 18% reduction. These findings imply that as the layer height increases, the ductility of the FDM PLA components also increases. Moreover, the FDM PLA-GO 0.15LH samples displayed a 20.7% reduction in area, compared to 20.9% for the FDM PLA-GO 0.3LH samples. These results suggest that incorporating graphene improved the ductility of the FDM PLA parts and should also improve the impact performance of FDM-GO parts.

4.7 Tensile fracture surface

Study of fracture surfaces provide an insight into the material failure modes and mechanisms. Therefore, SEM images were recorded from the fracture surfaces of tensile

PLA and PLA-GO samples. The tensile test results (Figure 4.8) showed that the highest TS was measured by the PLA-GO samples (PLA-GO 0.3LH - 50 MPa), while the lowest was recorded by the PLA samples (PLA 0.15LH - 42.4 MPa). In addition, analysis of printed PLA and PLA-GO samples show lack of any macro or microcracks in the PLA-GO 0.3LH (Figure 4.1.c) sample along with a uniform distribution of GO (Figure 4.2). This uniform distribution resulted in a part with the highest TS. On the other hand, PLA 0.15LH shows presence of microcracks and voids that resulted in defect induced failure resulting in the lowest TS. The presence of microcracks weakened the part and upon applying external loads, resulting in early failure.

Figure 4.9.a shows the presence of voids due to filament separation in the fracture surface of pure PLA 0.3LH. In contrast, the fracture surface (Figure 4.9.b) of PLA-GO sample (PLA-GO 0.15LH) shows lack of filament separation which led to presence of fewer voids after fracture. This resulted in a higher TS. Comparison of results for elongation at break for PLA and PLA-GO samples shows similar trends. The presence of voids in the fracture surface of PLA 0.3LH also resulted in lower ductility when compared to PLA-GO 0.15LH samples (Figure 4.9). In addition, the fractography images from the PLA samples show brittle failure on raster filaments from the central section while the skin (outer boundary) experience ductile fracture. This is due to the surface undulations present in the FDM samples that promote crack initiation on the surface which propagates to the center of the sample resulting in brittle failure.

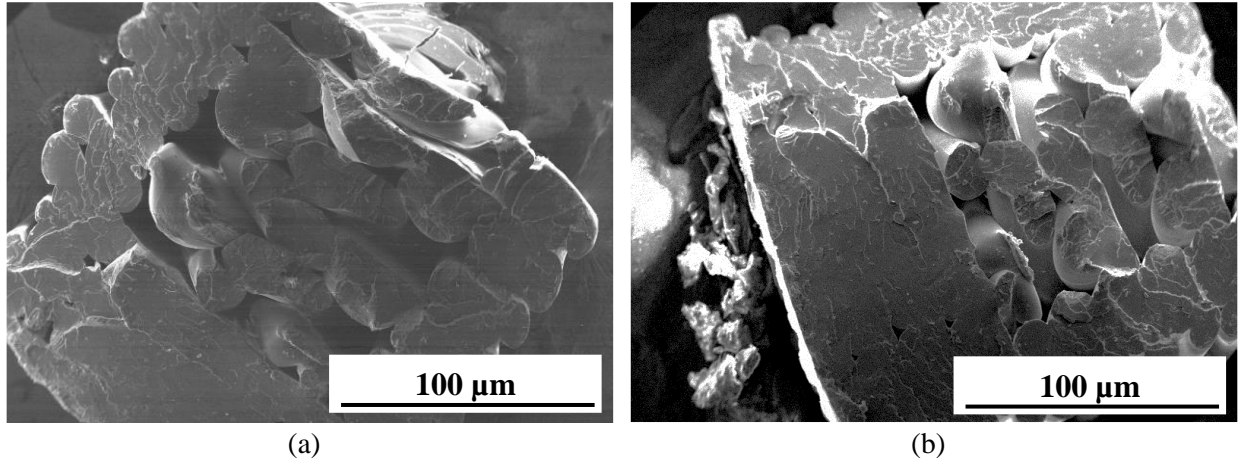


Figure 4.9: SEM Fracture surfaces, (a) PLA, (b) PLA-GO

4.8 Compression test

Compression tests are essential for understanding the materials response to compressive loads [137]. They help determine compressive properties (compressive strength, yield, and modulus), aiding in material selection and quality control for different applications. Figure 4.10 presents the compression test results for FDM PLA and PLA-GO samples, indicating that increasing layer height negatively affected FDM PLA's compression properties. Specifically, FDM PLA 0.15LH parts showed an average compressive strength of 207 MPa at 65% strain, a compressive YS of 75 MPa, and a compressive modulus of 2.25 GPa. In contrast, FDM PLA 0.3LH parts averaged a compressive strength of 200 MPa, a compressive YS of 62 MPa, and a compressive modulus of 2.05 GPa. These results signify a 3.5% decrease in compressive strength, a 17.3% reduction in YS, and an 8.9% decline in compressive modulus. Thus, the findings suggest an inverse correlation between layer height and the compressive strength and modulus of FDM PLA components.

The introduction of graphene enhanced the compressive strength of FDM PLA-GO 0.15LH parts. However, it also resulted in a reduction in compressive YS and modulus (Figure 4.10). Specifically, while the FDM PLA 0.15LH parts averaged a compressive strength of

207 MPa, a compressive YS of 75 MPa, and a compressive modulus of 2.25 GPa, the FDM PLA-GO 0.15LH samples showed an average compressive strength of 215 MPa, a compressive YS of 60 MPa, and a compressive modulus of 2.24 GPa. The results reveal that introducing GO led to a 22.7% increase in the compressive strength of FDM PLA 0.15LH parts, accompanied by a 20% reduction in compressive YS and a slight drop (0.4%) in their compressive modulus.

Furthermore, it has been reported that a higher graphene content enhances compressive properties due to graphene's exceptional bonding capabilities, fostering stronger interactions within the PLA matrix [104]. At 5 wt%, the highest compressive strength (96 MPa) and modulus (3.5 GPa) for PLA-GO were observed, while the lowest values of compressive strength (80 MPa) and modulus (2.6 GPa) were recorded at 0.5 wt% [104].

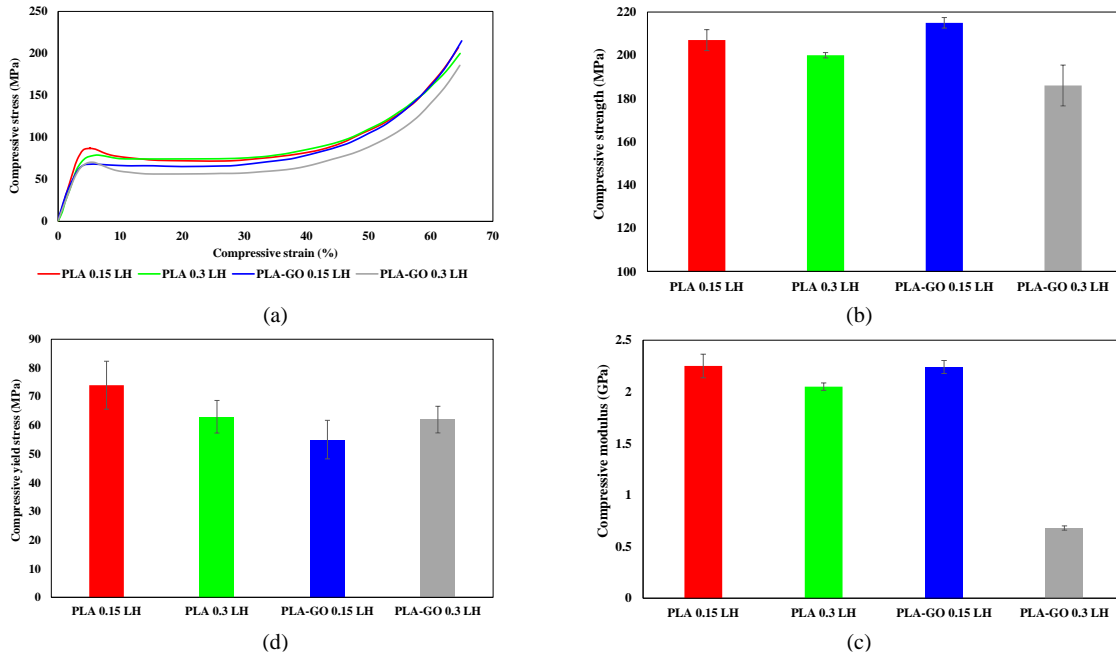


Figure 4.10: (a) Compression stress vs strain curves, (b) Compressive strength, (c) Compressive modulus, (d) Compressive yield stress

Conversely, the introduction of GO in the FDM PLA 0.3LH components resulted in a reduction in their compressive properties. While the FDM PLA 0.3LH parts showed an average compressive strength of 200 MPa, a compressive YS of 62 MPa, and a compressive modulus of 2.05 GPa, the FDM PLA-GO 0.3LH parts averaged a compressive strength of 186 MPa, a compressive YS of 60 MPa, and a compressive modulus of 0.68 GPa (Figure 4.10). This may be attributed to insufficient bonding between the graphene nanoparticles and the PLA matrix. Additionally, findings from another study indicate that incorporating graphene into PLA FDM parts led to reduction in compressive properties [94]. In their work, the PLA FDM parts achieved a compressive strength of 71.2 MPa with a compressive modulus of 2.02 GPa, whereas the PLA-graphene FDM parts measured a compressive strength of 64.4 MPa with a compressive modulus of 1.4 GPa [94].

4.9 Flexural test

The tensile and compressive properties provide a thorough analysis on the mechanical behavior of PLA and PLA-GO parts. However, uniaxial loading does not provide a complete set of mechanical properties. Bending tests, namely three-point and four-point, are often used to assess the material behavior under complex loading (tension-compression) as it provides the complete material response [137], [138]. In this work, PLA and PLA-GO samples were also tested under 3-point bending with varying layer heights.

The outcomes from the flexural tests are depicted in Figure 4.11 and indicate a clear effect of increased layer height on the flexural properties of FDM PLA parts. Specifically, the FDM PLA 0.15LH parts showed a flexural strength of 85.5 MPa and a flexural modulus of 3.2 GPa. With an elevation in layer height to 0.3 mm, PLA 0.3LH samples exhibited an increased flexural strength (by 2.1%) of 87.3 MPa, and the flexural modulus grew by 6.3%

to 3.4 GPa. Camargo et al. [99] noted a direct correlation between layer height and the flexural characteristics of FDM PLA parts. In their research, FDM PLA parts with a 0.27 mm layer height and 78% infill density displayed a flexural strength of 61 MPa and a flexural modulus of 2.5 GPa. In contrast, parts with a 0.13 mm layer height and 22% infill density achieved a flexural strength of 32 MPa and a flexural modulus of 1.5 GPa [99]. Notably, while FDM parts with larger layer heights displayed enhanced flexural properties, it is important to highlight that the infill density influenced the reported results. Higher infill density led to fewer voids, resulting in denser parts with superior properties [99].

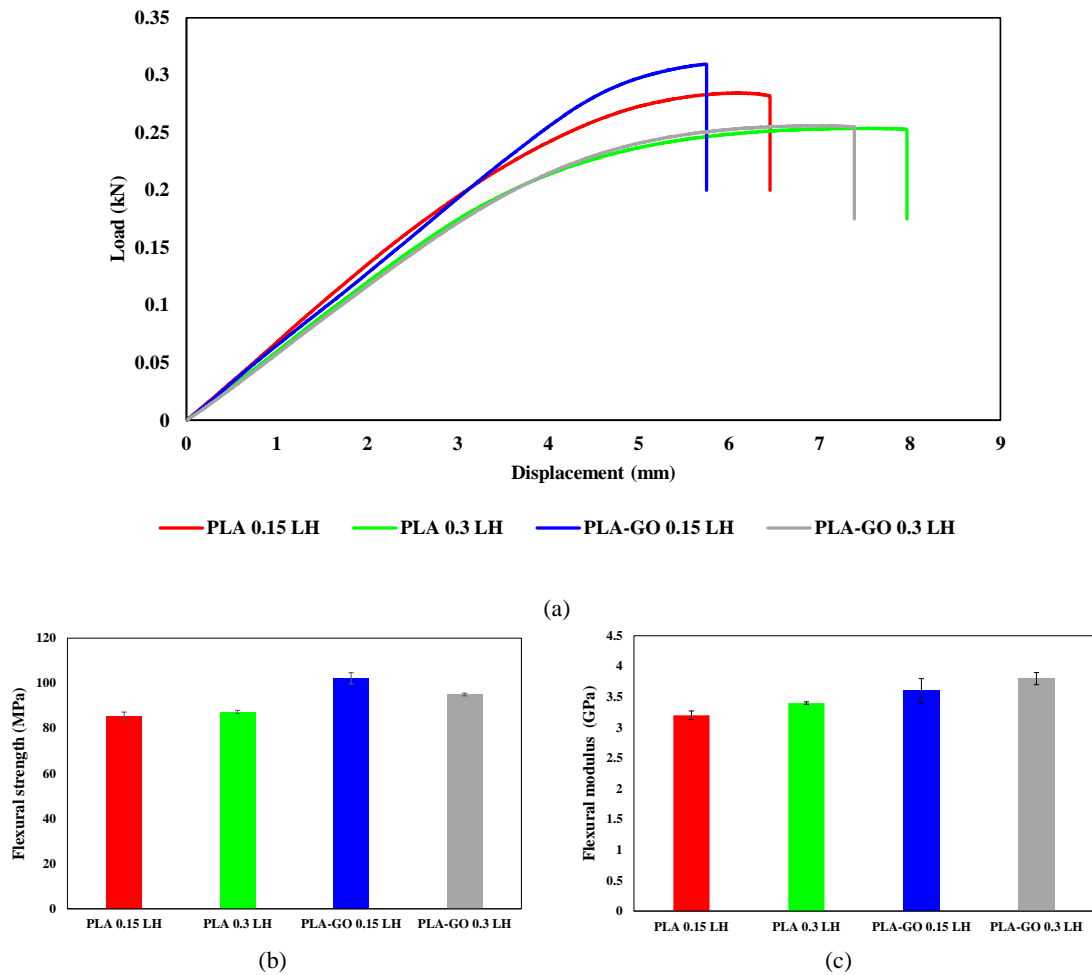


Figure 4.11: Flexural test results for PLA and PLA-GO samples (a) Force vs Displacement curves, (b) Flexural strength, (c) Flexural modulus

Furthermore, the FDM PLA-GO 0.15LH parts exhibited a flexural strength of 102.2 MPa and a flexural modulus of 3.6 GPa, while the FDM PLA-GO 0.3LH parts showed a flexural strength of 95 MPa and a flexural modulus of 3.8 GPa (Figure 4.11). The rise in layer height decreased the strength of PLA-GO samples by 7%. This might be due to the weaker adhesion between the PLA and GO nanoparticles in the 0.3 mm LH parts. This trend is in contrast with pure FDM PLA samples where the rise in layer height increased the flexural strength by 2.1%. Additionally, comparison of PLA (PLA 0.15LH) and PLA-GO (PLA-GO 0.15LH) samples showed a 19.5% increase in flexural strength PLA-GO samples.

In a similar study, it was found that FDM PLA-GO parts with a 2wt% composition achieved a flexural strength of 94.2 MPa and a flexural modulus of 3.07 GPa, while PLA parts showed a flexural strength of 79.2 MPa and a flexural modulus of 2.63 GPa [139]. However, their findings showed that FDM PLA exhibited superior flexural properties compared to PLA-GO parts with 0.5 and 1wt%. This was attributed to the unique properties and controlled distribution of the nanofiller within the PLA matrix [139].

Conversely, several studies indicated a decline in the flexural strength of PLA samples (83 MPa) upon the addition of graphene (78 MPa) [94], [103]. They reported a reduction of 6% in the flexural strength, attributed to inadequate dispersion of GO and its unique molecular geometry [94]. This resulted in a notable decrease in the maximum flexural stress with the inclusion of graphene [103]. However, it was noted that adding graphene to PLA FDM parts led to an increase in the flexural modulus [94]. Specifically, the FDM PLA-graphene parts achieved a flexural modulus of 2.09 GPa, while the PLA FDM parts recorded a flexural modulus of 2.03 GPa [94].

The flexural strengths observed in both PLA and PLA-GO samples suggests tensile dominated failures. Tensile test results (Figure 4.8) indicate failures beyond a minimum threshold of around 40 MPa for both PLA and PLA-GO parts. Thus, a flexural strength of 80 MPa would lead to failure on the surface under tensile loading. Surface analysis of flexural samples (Figure 4.12) clearly displays tensile failure due to asymmetric material response. In both FDM PLA and PLA-GO samples, failure occurred on the tensile surface due to crack initiation and propagation on the convex side, as the stresses exceeded the material's TS. Moreover, Figure 4.12 also illustrates how the rasters on the sample boundary acted as barriers, impeding crack propagation before eventual failure.

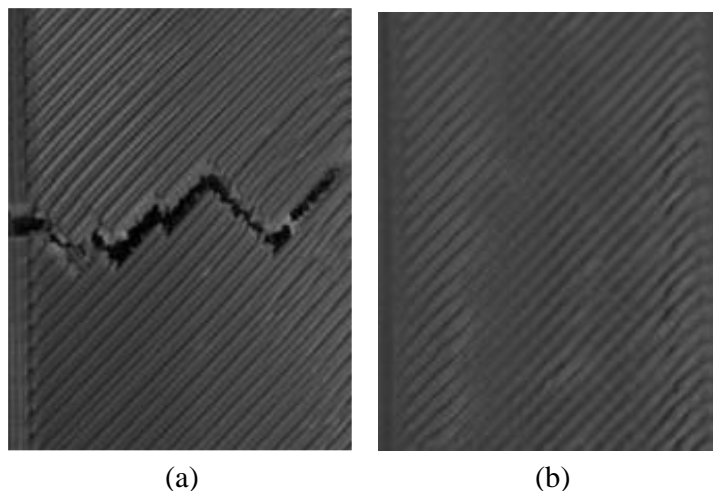


Figure 4.12: Fracture surface of flexural samples, (a) Top surface, (b) Bottom surface

4.10 Impact test

Tensile, compression, and flexure tests reveal how a material responds under static conditions, but understanding its behavior during impact, a dynamic situation, is equally vital [140]. Although GO has improved the static properties of PLA samples in this study (Section 4.6), its effect on dynamic properties needs further investigation. It is crucial to note that while enhancements in static performance are observed, superior impact

properties are not guaranteed, as factors such as ductility and surface area compared to cross-sectional area also influence impact behavior.

Figure 4.13 compiles the impact energy findings from both PLA and PLA-GO samples. The outcomes demonstrate a noticeable impact of the change in layer height on the impact energy of FDM parts. Specifically, the FDM PLA 0.15LH parts averaged an impact energy of 0.3 J, while the FDM PLA 0.3LH parts averaged 0.4 J, indicating a 16.2% enhancement in impact performance with an increase in layer height. This highlights a direct correlation between layer height and the impact energy of FDM samples. Plymill et al. [89] also carried out a study on FDM PLA samples and reported a maximum impact energy of approximately 0.2 J.

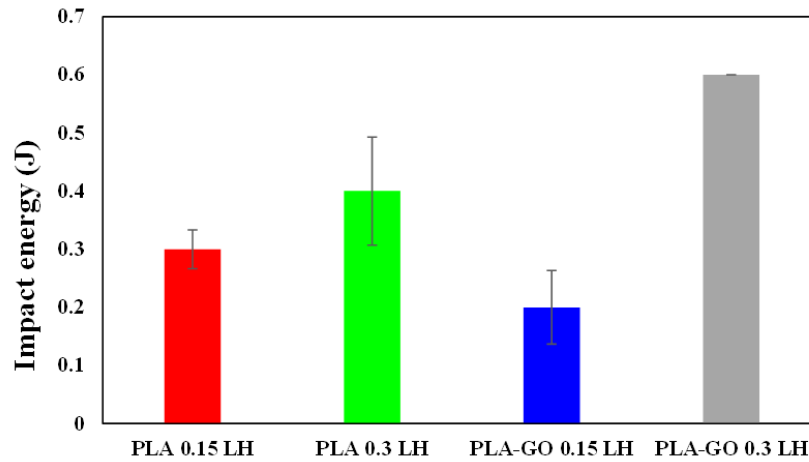


Figure 4.13: Impact test results

Based on the findings in Figure 4.13, adding graphene had a diverse impact on the impact energy of FDM PLA samples. The FDM PLA-GO 0.15LH samples exhibited an impact energy of 0.2 J, reflecting a 50% decrease, while the FDM PLA-GO 0.3LH parts showcased an impact energy of 0.6 J, resulting in a 50% increase. These results imply that altering the layer height within the PLA-GO parts influences interlayer bonding. A related

study observed a decrease in impact energy with PLA-GO samples [94]. Vidakis et al. [94] concluded that incorporating graphene led to a 31.4% reduction in the impact energy of FDM PLA samples.

In contrast, Plymill et al. [89] found that introducing graphene (at 0.2 wt%) enhanced the impact energy of FDM PLA samples by nearly 12% [89]. This distinction between PLA and PLA-GO samples could be attributed to optimal parameters and adjusting the filler volume fraction in PLA parts. Plymill et al. [89] also investigated the impact of filler volume fraction, noting that a 0.1 wt% graphene showed no change in impact energy, while a 0.5 wt% demonstrated a slight increase. However, the most significant enhancement (11.7%) in the impact energy of FDM PLA parts occurred when employing a 0.2 wt% graphene concentration [89].

4.11 Hardness test

Rockwell and Vickers hardness tests are essential for assessing material hardness. Rockwell tests measure indentation depth swiftly and suit various materials [141]. The Vickers tests provides accurate and reliable microhardness readings, making it valuable for evaluating the hardness of small or intricate materials [142]. Figure 4.14.a outlines the Rockwell-R hardness test results obtained from the PLA and PLA-GO samples. The data suggests that lower layer heights correlated with higher hardness, showing an increase of 8.2%. Specifically, the FDM PLA 0.15LH parts displayed a hardness of 98 HRR, whereas the FDM PLA 0.3LH parts indicated a hardness of 90 HRR.

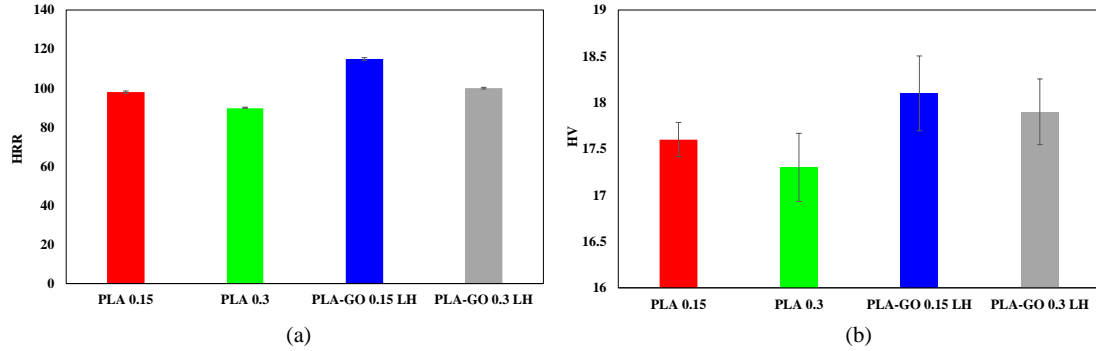


Figure 4.14: (a) Rockwell-R hardness results and (b) Vickers micro hardness test results

Furthermore, the inclusion of GO within the PLA matrix elevated the HRR hardness of both PLA and PLA-GO parts by 11.1% and 17.3%, respectively (Figure 4.14.a). Unlike the FDM PLA samples, the hardness of the PLA-GO samples decreased with increased layer thickness. Vidakis et al. [94] conducted a similar study, reporting a hardness of 98 HRR for pure FDM PLA samples and 100 HRR for the PLA-GO parts.

Figure 4.14.b outlines the Vickers micro hardness findings for both PLA and PLA-GO samples. Similar to the HRR results, lower layer height correlated with higher micro hardness. For example, the FDM PLA 0.15LH samples exhibited a micro hardness of 17.6 HV, while the PLA 0.3LH parts showed a slightly lower micro hardness of 17.3 HV (a decrease of 1.7%). Similarly, the PLA-GO samples displayed higher hardness compared to PLA samples, with a 2.8% increase for the 0.15LH samples and a 3.5% increase for the 0.3LH parts. Specifically, the FDM PLA-GO 0.15LH samples indicated a micro hardness of 18.1 HV, while the FDM PLA-GO 0.3LH achieved a micro hardness of 17.9 HV. However, these minor alterations in micro hardness resulting from changes in layer height and the addition of GO do not suggest a significant overall rise.

On the other hand, Vidakis et al. [94] observed a clear enhancement in micro hardness due to graphene. They noted FDM PLA samples showing 16.7 HV in micro hardness, while

FDM PLA graphene samples exhibited notably higher micro hardness at 9.6 HV [94]. These differences might be due to varied FDM process parameters and methods for preparing FDM nanocomposites. Additionally, the appearance of aggregates within the PLA structure might also contribute to these variations. Poor dispersion of graphene is known to result in aggregate formation, leading to reduced micro hardness values [106]. It is important to note that error bars for HV exhibit higher deviation than HRR results due to increased variability observed in micro hardness measurements. This higher variability can stem from inconsistencies during material preparation or testing conditions.

The experimental observations attained from the PLA and PLA-GO parts highlight the importance of several factors (Figure 4.15). If the PLA matrix was not bonded properly to the GO nanoparticles, it would lead to lower strength. Similarly, agglomerated GO nanoparticles would act as stress raisers leading to lower strength due to layer adhesion and debonding issues (Figure 4.15.a). Uniformly distributed GO nanoparticles would reduce this effect (Figure 4.15.b). However, as the layer height is a major factor in establishing the mechanical properties of PLA and PLA-GO parts, careful examination is required to assess the effect of agglomeration and uniform distribution in FDM PLA and PLA-GO parts.

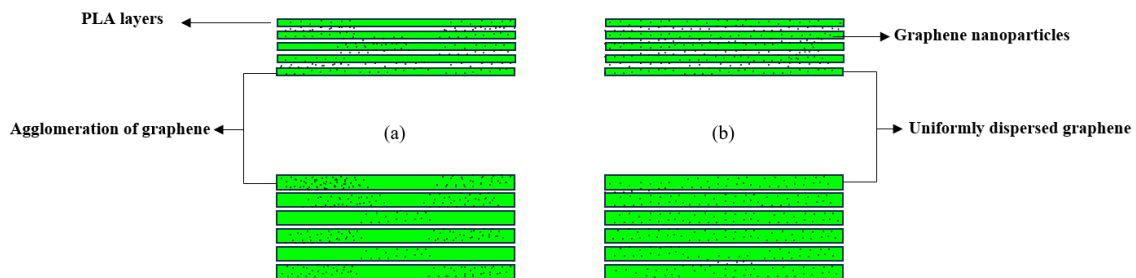


Figure 4.15: Dispersion of graphene in PLA (a) Agglomerated, (b) Uniform dispersion

CHAPTER 5

CONCLUSIONS

In conclusion, in this thesis, pure FDM PLA parts were compared to FDM PLA-GO parts. The GO was added using an in-situ nozzle impregnation technique. The mechanical and thermal properties of the FDM processed parts were thoroughly investigated at varying layer heights. Through a rigorous experimental approach, this study illuminated the multifaceted impact of graphene oxide on these key material properties.

FDM PLA and PLA-GO parts were characterized using TGA and the results pointed that the degradation temperature of FDM PLA parts and the residual wt% increased with the addition of GO. In addition, the TGA results confirm that 1 wt% of GO was used as nanofiller in the FDM PLA-GO parts. DSC was also performed to compare the thermal transitions between PLA and PLA-GO samples. Results showed that the integration of GO resulted in the reduction of the T_g (by 0.5 %) and X_c % (by 22.9 %) of PLA parts. Conversely, the T_m increased slightly from 148.8°C to 148.9°C. The XRD results interpreted that the characteristic peaks were located at similar diffraction angles for both the FDM PLA and PLA-GO parts. However, broader peaks were recorded by the FDM PLA-GO parts. Similar to DSC results, broader peaks indicate a reduction in crystallinity. The FTIR results showed that the distinct peaks that were observed by the FDM PLA-GO parts at 3434, 2362 and 1627 cm⁻¹ were due to the intermolecular interactions caused by GO, while other peaks depicted in the FTIR results were mutual between the FDM PLA and FDM PLA-GO parts.

Tensile, compressive, flexural, impact and hardness of the PLA and PLA-GO samples were also analyzed to assess the influence of graphene oxide on the mechanical properties of PLA-GO parts. The mechanical test results revealed that the change in layer height and addition of GO had a noticeable effect on the mechanical properties of the FDM PLA parts. The tensile test results indicated that the FDM PLA 0.3LH parts achieved a higher TS (43.5 MPa) and modulus (2.9 GPa) with a lower elongation at break (4.1%) compared to the FDM PLA 0.15LH parts. The integration of GO enhanced the tensile properties of the FDM PLA 0.3LH parts, while the FDM PLA 0.15LH parts exhibited an increase in their TS (48.5 MPa) and modulus (2.7 GPa) with a slight reduction in the elongation at break (4.8%) with the incorporation of GO.

SEM images from the fracture surfaces of tensile samples were also analyzed to study the differences between PLA and PLA-GO samples. SEM results showed the presence of GO nanoparticles between the deposited PLA layers. The compression test results showed that the FDM PLA 0.3LH parts achieved lower compressive properties (200 MPa compressive strength at 65% strain) compared to the 0.15mm layer height (207 MPa compressive strength at 65% strain) parts. The presence of GO increased the compressive strength of the FDM PLA parts while resulting in a lower compressive YS and modulus.

The flexural test findings showed that the flexural strength and modulus of the FDM PLA parts improved with the growth in layer height from 0.15 to 0.3 mm by 7% and 5.6%, respectively. The flexural strength and modulus were also enhanced with the addition of GO by 19.5% and 12.5% for the FDM PLA-GO 0.15LH parts, respectively. However, the FDM PLA-GO 0.15LH parts recorded higher flexural properties compared to the FDM PLA-GO 0.3LH parts. The impact test results illustrated that the impact energies recorded

by the FDM PLA parts increased by 16.2% with the increase in layer height. Furthermore, at the same layer height, the addition of GO resulted in a 50% increase in the impact energy for the FDM PLA 0.3LH samples, while leading to a 50% decrease in the impact energies recorded by the FDM PLA-GO 0.15LH samples.

Macro and micro Hardness tests were also conducted to analyze the effect of the layer height and GO on the FDM PLA parts. The macro and micro hardness results depicted that the hardness of the FDM PLA parts decreased by 8.2% (0.15LH) and 1.7% (0.3LH) with an increase in layer height, while the addition of GO enhanced the hardness of the FDM PLA parts by 17.3% (0.15LH) and 2.84% (0.3LH) for the FDM PLA-GO 0.15LH parts.

The comprehensive analyses performed in this work has yielded a rich dataset, contributing to an improved understanding of the interplay between the addition of GO and the resultant material properties using a novel in-situ nozzle impregnation approach. In addition, these findings not only enhance our knowledge of PLA-GO composites but also offer valuable insights for optimizing their formulation in FDM applications. Ultimately, this research sets the stage for advancements in additive manufacturing processes, easing the path for the development of high-performance PLA-GO composites with superior properties tailored for specific applications.

REFERENCES

- [1] M. Javaid, A. Haleem, R. P. Singh, R. Suman, and E. S. Gonzalez, “Understanding the adoption of Industry 4.0 technologies in improving environmental sustainability,” *Sustainable Operations and Computers*, vol. 3, pp. 203–217, 2022, doi: 10.1016/j.susoc.2022.01.008.
- [2] S. Rouf *et al.*, “Additive manufacturing technologies: Industrial and medical applications,” *Sustainable Operations and Computers*, vol. 3, pp. 258–274, 2022, doi: 10.1016/j.susoc.2022.05.001.
- [3] F. Calignano and V. Mercurio, “An overview of the impact of additive manufacturing on supply chain, reshoring, and sustainability,” *Cleaner Logistics and Supply Chain*, vol. 7, p. 100103, Jun. 2023, doi: 10.1016/j.clscn.2023.100103.
- [4] F. P. W. Melchels, J. Feijen, and D. W. Grijpma, “A review on stereolithography and its applications in biomedical engineering,” *Biomaterials*, vol. 31, no. 24, pp. 6121–6130, Aug. 2010, doi: 10.1016/j.biomaterials.2010.04.050.
- [5] B. Duan and M. Wang, “Selective laser sintering and its application in biomedical engineering,” *MRS Bull*, vol. 36, no. 12, pp. 998–1005, Dec. 2011, doi: 10.1557/mrs.2011.270.
- [6] R. P. Rimington, A. J. Capel, S. D. R. Christie, and M. P. Lewis, “Biocompatible 3D printed polymers via fused deposition modelling direct C₂C₁₂ cellular phenotype in vitro,” *Lab Chip*, vol. 17, no. 17, pp. 2982–2993, 2017, doi: 10.1039/C7LC00577F.

- [7] P. A. Webb, "A review of rapid prototyping (RP) techniques in the medical and biomedical sector," *J Med Eng Technol*, vol. 24, no. 4, pp. 149–153, Jan. 2000, doi: 10.1080/03091900050163427.
- [8] G. D. Goh, S. Agarwala, G. L. Goh, V. Dikshit, S. L. Sing, and W. Y. Yeong, "Additive manufacturing in unmanned aerial vehicles (UAVs): Challenges and potential," *Aerosp Sci Technol*, vol. 63, pp. 140–151, Apr. 2017, doi: 10.1016/j.ast.2016.12.019.
- [9] G. L. Goh, S. Agarwala, and W. Y. Yeong, "Directed and On-Demand Alignment of Carbon Nanotube: A Review toward 3D Printing of Electronics," *Adv Mater Interfaces*, vol. 6, no. 4, Feb. 2019, doi: 10.1002/admi.201801318.
- [10] J. C. Vasco, "Additive manufacturing for the automotive industry," in *Additive Manufacturing*, Elsevier, 2021, pp. 505–530. doi: 10.1016/B978-0-12-818411-0.00010-0.
- [11] *3D Bioprinting for Reconstructive Surgery*. Elsevier, 2018. doi: 10.1016/C2015-0-06000-2.
- [12] C. Lubombo and M. A. Huneault, "Effect of infill patterns on the mechanical performance of lightweight 3D-printed cellular PLA parts," *Mater Today Commun*, vol. 17, pp. 214–228, Dec. 2018, doi: 10.1016/J.MTCOMM.2018.09.017.
- [13] M. S. Alsoufi *et al.*, "Experimental Characterization of the Influence of Nozzle Temperature in FDM 3D Printed Pure PLA and Advanced PLA+," *American*

- Journal of Mechanical Engineering*, vol. 7, no. 2, pp. 45–60, Apr. 2019, doi:
10.12691/ajme-7-2-1.
- [14] A. Nasirov and I. Fidan, “Prediction of mechanical properties of fused filament fabricated structures via asymptotic homogenization,” *Mechanics of Materials*, vol. 145, Jun. 2020, doi: 10.1016/j.mechmat.2020.103372.
- [15] T. N. A. T. Rahim, A. M. Abdullah, and H. Md Akil, “Recent Developments in Fused Deposition Modeling-Based 3D Printing of Polymers and Their Composites,” *Polymer Reviews*, vol. 59, no. 4, pp. 589–624, Oct. 2019, doi: 10.1080/15583724.2019.1597883.
- [16] R. B. Kristiawan, F. Imaduddin, D. Ariawan, Ubaidillah, and Z. Arifin, “A review on the fused deposition modeling (FDM) 3D printing: Filament processing, materials, and printing parameters,” *Open Engineering*, vol. 11, no. 1. De Gruyter Open Ltd, pp. 639–649, Jan. 01, 2021. doi: 10.1515/eng-2021-0063.
- [17] P. K. Penumakala, J. Santo, and A. Thomas, “A critical review on the fused deposition modeling of thermoplastic polymer composites,” *Composites Part B: Engineering*, vol. 201. Elsevier Ltd, Nov. 15, 2020. doi: 10.1016/j.compositesb.2020.108336.
- [18] V. Guerra, C. Wan, and T. McNally, “Fused deposition modelling (FDM) of composites of graphene nanoplatelets and polymers for high thermal conductivity: a mini-review,” *Functional Composite Materials*, vol. 1, no. 1, Dec. 2020, doi: 10.1186/s42252-020-00005-x.

- [19] H. Belaid *et al.*, “Development of new biocompatible 3D printed graphene oxide-based scaffolds,” *Materials Science and Engineering C*, vol. 110, May 2020, doi: 10.1016/j.msec.2019.110595.
- [20] D. Zhang *et al.*, “Fabrication of highly conductive graphene flexible circuits by 3D printing,” *Synth Met*, vol. 217, pp. 79–86, Jul. 2016, doi: 10.1016/j.synthmet.2016.03.014.
- [21] X. Wei *et al.*, “3D Printable Graphene Composite,” *Sci Rep*, vol. 5, Jul. 2015, doi: 10.1038/srep11181.
- [22] Q. Chen, J. D. Mangadlao, J. Wallat, A. De Leon, J. K. Pokorski, and R. C. Advincula, “3D printing biocompatible polyurethane/poly(lactic acid)/graphene oxide nanocomposites: Anisotropic properties,” *ACS Appl Mater Interfaces*, vol. 9, no. 4, pp. 4015–4023, 2017, doi: 10.1021/acsami.6b11793.
- [23] H. Wu, L. Liu, Y. Cai, P. Qian, C. Zhang, and B. Li, “A novel gradient graphene composite with broadband microwave absorption fabricated by fused deposition modelling,” *Materials Technology*, vol. 37, no. 4, pp. 280–287, 2022, doi: 10.1080/10667857.2020.1837487.
- [24] H. Lu, “Preliminary mechanical characterization of the low-cost metal 3D printing,” Tennessee Technological University, 2020.
- [25] J. Beniak, L. Šooš, P. Križan, M. Matúš, and V. Ruprich, “Resistance and Strength of Conductive PLA Processed by FDM Additive Manufacturing,” *Polymers (Basel)*, vol. 14, no. 4, 2022, doi: 10.3390/polym14040678.

- [26] A. Chalgham, A. Ehrmann, and I. Wickenkamp, “Mechanical properties of fdm printed pla parts before and after thermal treatment,” *Polymers (Basel)*, vol. 13, no. 8, 2021, doi: 10.3390/polym13081239.
- [27] A. el Moumen, M. Tarfaoui, and K. Lafdi, “Additive manufacturing of polymer composites: Processing and modeling approaches,” *Compos B Eng*, vol. 171, pp. 166–182, Aug. 2019, doi: 10.1016/j.compositesb.2019.04.029.
- [28] Y. A. Jin, H. Li, Y. He, and J. Z. Fu, “Quantitative analysis of surface profile in fused deposition modelling,” *Addit Manuf*, vol. 8, pp. 142–148, Oct. 2015, doi: 10.1016/j.addma.2015.10.001.
- [29] M. Li, W. Du, A. Elwany, Z. Pei, and C. Ma, “Metal Binder Jetting Additive Manufacturing: A Literature Review,” *J Manuf Sci Eng*, vol. 142, no. 9, Sep. 2020, doi: 10.1115/1.4047430.
- [30] P. K. Gokuldoss, S. Kolla, and J. Eckert, “Additive Manufacturing Processes: Selective Laser Melting, Electron Beam Melting and Binder Jetting—Selection Guidelines,” *Materials*, vol. 10, no. 6, p. 672, Jun. 2017, doi: 10.3390/ma10060672.
- [31] M. Ziaee and N. B. Crane, “Binder jetting: A review of process, materials, and methods,” *Addit Manuf*, vol. 28, pp. 781–801, Aug. 2019, doi: 10.1016/j.addma.2019.05.031.

- [32] T. Moritz and S. Maleksaeedi, “Additive manufacturing of ceramic components,” in *Additive Manufacturing*, Elsevier, 2018, pp. 105–161. doi: 10.1016/B978-0-12-812155-9.00004-9.
- [33] J. Z. Manapat, Q. Chen, P. Ye, and R. C. Advincula, “3D Printing of Polymer Nanocomposites via Stereolithography,” *Macromol Mater Eng*, vol. 302, no. 9, Sep. 2017, doi: 10.1002/mame.201600553.
- [34] M. Mukhtarkhanov, A. Perveen, and D. Talamona, “Application of Stereolithography Based 3D Printing Technology in Investment Casting,” *Micromachines (Basel)*, vol. 11, no. 10, p. 946, Oct. 2020, doi: 10.3390/mi11100946.
- [35] A. Razavykia, E. Brusa, C. Delprete, and R. Yavari, “An Overview of Additive Manufacturing Technologies—A Review to Technical Synthesis in Numerical Study of Selective Laser Melting,” *Materials*, vol. 13, no. 17, p. 3895, Sep. 2020, doi: 10.3390/ma13173895.
- [36] J. Kruth, P. Mercelis, J. Van Vaerenbergh, L. Froyen, and M. Rombouts, “Binding mechanisms in selective laser sintering and selective laser melting,” *Rapid Prototyp J*, vol. 11, no. 1, pp. 26–36, Feb. 2005, doi: 10.1108/13552540510573365.
- [37] J. P. Kruth, X. Wang, T. Laoui, and L. Froyen, “Lasers and materials in selective laser sintering,” *Assembly Automation*, vol. 23, no. 4, pp. 357–371, Dec. 2003, doi: 10.1108/01445150310698652.

- [38] R. Ganeriwala and T. I. Zohdi, “A coupled discrete element-finite difference model of selective laser sintering,” *Granul Matter*, vol. 18, no. 2, p. 21, May 2016, doi: 10.1007/s10035-016-0626-0.
- [39] C. Y. Yap *et al.*, “Review of selective laser melting: Materials and applications,” *Appl Phys Rev*, vol. 2, no. 4, Dec. 2015, doi: 10.1063/1.4935926.
- [40] V. V. Popov *et al.*, “Design and 3D-printing of titanium bone implants: brief review of approach and clinical cases,” *Biomed Eng Lett*, vol. 8, no. 4, pp. 337–344, Nov. 2018, doi: 10.1007/s13534-018-0080-5.
- [41] J. Park, M. J. Tari, and H. T. Hahn, “Characterization of the laminated object manufacturing (LOM) process,” *Rapid Prototyp J*, vol. 6, no. 1, pp. 36–50, Mar. 2000, doi: 10.1108/13552540010309868.
- [42] A. Gebhardt, *Understanding additive manufacturing : rapid prototyping, rapid tooling, rapid manufacturing*. Hanser Publishers, 2012.
- [43] Rajan K, Mahendran S, Kumaran K, Devarajan R, Ngui W.K, and Adarsh K.P, “3D Printing Technology for Thermal Application: A Brief Review,” *Journal of Advanced Research in Fluid Mechanics and Thermal Sciences*, vol. 83, no. 2, pp. 84–97, Jun. 2021, doi: 10.37934/arfmts.83.2.8497.
- [44] A. Saboori, A. Aversa, G. Marchese, S. Biamino, M. Lombardi, and P. Fino, “Application of Directed Energy Deposition-Based Additive Manufacturing in Repair,” *Applied Sciences*, vol. 9, no. 16, p. 3316, Aug. 2019, doi: 10.3390/app9163316.

- [45] J. C. Heigel, P. Michaleris, and E. W. Reutzel, “Thermo-mechanical model development and validation of directed energy deposition additive manufacturing of Ti-6Al-4V,” *Addit Manuf*, vol. 5, pp. 9–19, Jan. 2015, doi: 10.1016/j.addma.2014.10.003.
- [46] R. Shah, N. Pai, A. Rosenkranz, K. Shirvani, and M. Marian, “Tribological Behavior of Additively Manufactured Metal Components,” *Journal of Manufacturing and Materials Processing*, vol. 6, no. 6, p. 138, Nov. 2022, doi: 10.3390/jmmp6060138.
- [47] Y. L. Yap, C. Wang, S. L. Sing, V. Dikshit, W. Y. Yeong, and J. Wei, “Material jetting additive manufacturing: An experimental study using designed metrological benchmarks,” *Precis Eng*, vol. 50, pp. 275–285, Oct. 2017, doi: 10.1016/j.precisioneng.2017.05.015.
- [48] A. Elkaseer, K. J. Chen, J. C. Janhsen, O. Refle, V. Hagenmeyer, and S. G. Scholz, “Material jetting for advanced applications: A state-of-the-art review, gaps and future directions,” *Addit Manuf*, vol. 60, p. 103270, Dec. 2022, doi: 10.1016/j.addma.2022.103270.
- [49] O. Gülcan, K. Günaydın, and A. Tamer, “The State of the Art of Material Jetting—A Critical Review,” *Polymers (Basel)*, vol. 13, no. 16, p. 2829, Aug. 2021, doi: 10.3390/polym13162829.
- [50] M. Sireesha, J. Lee, A. S. Kranthi Kiran, V. J. Babu, B. B. T. Kee, and S. Ramakrishna, “A review on additive manufacturing and its way into the oil and

- gas industry,” *RSC Adv*, vol. 8, no. 40, pp. 22460–22468, 2018, doi:
10.1039/C8RA03194K.
- [51] A. Mahmood, T. Akram, H. Chen, and S. Chen, “On the Evolution of Additive Manufacturing (3D/4D Printing) Technologies: Materials, Applications, and Challenges,” *Polymers*, vol. 14, no. 21. MDPI, Nov. 01, 2022. doi:
10.3390/polym14214698.
- [52] S. Arabnejad, B. Johnston, M. Tanzer, and D. Pasini, “Fully porous 3D printed titanium femoral stem to reduce stress-shielding following total hip arthroplasty,” *Journal of Orthopaedic Research*, vol. 35, no. 8, pp. 1774–1783, Aug. 2017, doi:
10.1002/jor.23445.
- [53] M. Petch, “Audi gives update on use of SLM metal 3D printing for the automotive industry.” Accessed: Dec. 26, 2023. [Online]. Available:
<https://3dprintingindustry.com/news/audi-gives-update-use-slm-metal-3d-printing-automotive-industry-129376/>
- [54] L. Mohon, “NASA Advances Additive Manufacturing For Rocket Propulsion.” Accessed: Dec. 26, 2023. [Online]. Available:
<https://www.nasa.gov/technology/manufacturing-materials-3-d-printing/nasa-advances-additive-manufacturing-for-rocket-propulsion/>
- [55] S. Guo, K. Qiu, F. Meng, S. H. Park, and M. C. McAlpine, “3D Printed Stretchable Tactile Sensors,” *Advanced Materials*, vol. 29, no. 27, Jul. 2017, doi:
10.1002/adma.201701218.

- [56] P. Wu, J. Wang, and X. Wang, “A critical review of the use of 3-D printing in the construction industry,” *Autom Constr*, vol. 68, pp. 21–31, Aug. 2016, doi: 10.1016/j.autcon.2016.04.005.
- [57] G. Kannayiram, S. Sendilvelan, and M. P. R., “Importance of nanocomposites in 3D bioprinting: An overview,” *Bioprinting*, vol. 32, p. e00280, Jul. 2023, doi: 10.1016/j.bprint.2023.e00280.
- [58] F. D. Al-Shalawi *et al.*, “Biomaterials as Implants in the Orthopedic Field for Regenerative Medicine: Metal versus Synthetic Polymers,” *Polymers (Basel)*, vol. 15, no. 12, p. 2601, Jun. 2023, doi: 10.3390/polym15122601.
- [59] N. Zhao *et al.*, “Direct additive manufacturing of metal parts for automotive applications,” *J Manuf Syst*, vol. 68, pp. 368–375, Jun. 2023, doi: 10.1016/j.jmsy.2023.04.008.
- [60] S. Salifu, D. Desai, O. Ogunbiyi, and K. Mwale, “Recent development in the additive manufacturing of polymer-based composites for automotive structures—a review,” *The International Journal of Advanced Manufacturing Technology*, vol. 119, no. 11–12, pp. 6877–6891, Apr. 2022, doi: 10.1007/s00170-021-08569-z.
- [61] A. Angrish, “A critical analysis of additive manufacturing technologies for aerospace applications,” in *2014 IEEE Aerospace Conference*, IEEE, Mar. 2014, pp. 1–6. doi: 10.1109/AERO.2014.6836456.
- [62] J. C. Najmon, S. Raeisi, and A. Tovar, “Review of additive manufacturing technologies and applications in the aerospace industry,” in *Additive*

- Manufacturing for the Aerospace Industry*, Elsevier, 2019, pp. 7–31. doi:
10.1016/B978-0-12-814062-8.00002-9.
- [63] Lucas Mearian, “Boeing turns to 3D-printed parts to save millions on its 787 Dreamliner.” Accessed: Dec. 04, 2023. [Online]. Available:
<https://www.computerworld.com/article/3188899/boeing-turns-to-3d-printed-parts-to-save-millions-on-its-787-dreamliner.html>
- [64] C. H. Rao, K. Avinash, B. K. S. V. L. Varaprasad, and S. Goel, “A Review on Printed Electronics with Digital 3D Printing: Fabrication Techniques, Materials, Challenges and Future Opportunities,” *J Electron Mater*, vol. 51, no. 6, pp. 2747–2765, Jun. 2022, doi: 10.1007/s11664-022-09579-7.
- [65] A. H. Espera, J. R. C. Dizon, Q. Chen, and R. C. Advincula, “3D-printing and advanced manufacturing for electronics,” *Progress in Additive Manufacturing*, vol. 4, no. 3, pp. 245–267, Sep. 2019, doi: 10.1007/s40964-019-00077-7.
- [66] X. Wang, M. Jiang, Z. Zhou, J. Gou, and D. Hui, “3D printing of polymer matrix composites: A review and prospective,” *Composites Part B: Engineering*, vol. 110. Elsevier Ltd, pp. 442–458, Feb. 01, 2017. doi: 10.1016/j.compositesb.2016.11.034.
- [67] J. Nilimaa, “Smart materials and technologies for sustainable concrete construction,” *Developments in the Built Environment*, vol. 15, p. 100177, Oct. 2023, doi: 10.1016/j.dibe.2023.100177.

- [68] M. Bazli, H. Ashrafi, A. Rajabipour, and C. Kutay, “3D printing for remote housing: Benefits and challenges,” *Autom Constr*, vol. 148, p. 104772, Apr. 2023, doi: 10.1016/j.autcon.2023.104772.
- [69] T. Rayna and L. Striukova, “From rapid prototyping to home fabrication: How 3D printing is changing business model innovation,” *Technol Forecast Soc Change*, vol. 102, pp. 214–224, Jan. 2016, doi: 10.1016/j.techfore.2015.07.023.
- [70] R. Mandala, A. P. Bannoth, S. Akella, V. K. Rangari, and D. Kodali, “A short review on fused deposition modeling 3D printing of bio-based polymer nanocomposites,” *J Appl Polym Sci*, vol. 139, no. 14, pp. 1–19, 2022, doi: 10.1002/app.51904.
- [71] S. Wickramasinghe, T. Do, and P. Tran, “FDM-Based 3D printing of polymer and associated composite: A review on mechanical properties, defects and treatments,” *Polymers*, vol. 12, no. 7. MDPI AG, pp. 1–42, Jul. 01, 2020. doi: 10.3390/polym12071529.
- [72] D. Vaes and P. Van Puyvelde, “Semi-crystalline feedstock for filament-based 3D printing of polymers,” *Prog Polym Sci*, vol. 118, p. 101411, Jul. 2021, doi: 10.1016/j.progpolymsci.2021.101411.
- [73] J. P. Greene, “Microstructures of Polymers,” in *Automotive Plastics and Composites*, Elsevier, 2021, pp. 27–37. doi: 10.1016/B978-0-12-818008-2.00009-X.

- [74] Ultimaker, "Ultimaker PLA Technical Datasheet," Apr. 2022. Accessed: Dec. 27, 2023. [Online]. Available: <https://ultimaker.com/materials/>
- [75] Ultimaker, "Ultimaker ABS Technical Datasheet," Apr. 2022. Accessed: Dec. 27, 2023. [Online]. Available: <https://ultimaker.com/materials/>
- [76] Ultimaker, "Ultimaker PVA Technical Datasheet," Apr. 2022. Accessed: Dec. 27, 2023. [Online]. Available: <https://ultimaker.com/materials/>
- [77] 3D4MAKERS, "PEEK Filament." [Online]. Available: www.3d4makers.com
- [78] Ultimaker, "Ultimaker PETG Technical Datasheet," Apr. 2022. Accessed: Dec. 27, 2023. [Online]. Available: <https://ultimaker.com/materials/>
- [79] Ultimaker, "Ultimaker Nylon Technical Datasheet," Apr. 2022. Accessed: Dec. 27, 2023. [Online]. Available: <https://ultimaker.com/materials/>
- [80] Ultimaker, "Ultimaker PP Technical Datasheet," Apr. 2022. Accessed: Dec. 27, 2023. [Online]. Available: <https://ultimaker.com/materials/>
- [81] BASF, "BASF 3D Printing Solutions BV sales@basf-3dps.com www.basf-3dps.com General information." [Online]. Available: www.basf-3dps.com
- [82] Ultimaker, "Ultimaker PC Technical Datasheet," Apr. 2022. Accessed: Dec. 27, 2023. [Online]. Available: <https://ultimaker.com/materials/>
- [83] Ultimaker, "Ultimaker TPU 95A Technical Datasheet," Apr. 2022. Accessed: Dec. 27, 2023. [Online]. Available: <https://ultimaker.com/materials/>

- [84] M. Heidari-Rarani, N. Ezati, P. Sadeghi, and M. Badrossamay, "Optimization of FDM process parameters for tensile properties of polylactic acid specimens using Taguchi design of experiment method," *Journal of Thermoplastic Composite Materials*, vol. 35, no. 12, pp. 2435–2452, Dec. 2022, doi: 10.1177/0892705720964560.
- [85] D. K. Rajak, D. D. Pagar, R. Kumar, and C. I. Pruncu, "Recent progress of reinforcement materials: a comprehensive overview of composite materials," *Journal of Materials Research and Technology*, vol. 8, no. 6, pp. 6354–6374, Nov. 2019, doi: 10.1016/j.jmrt.2019.09.068.
- [86] A. Dey, I. N. R. Eagle, and N. Yodo, "A review on filament materials for fused filament fabrication," *Journal of Manufacturing and Materials Processing*, vol. 5, no. 3. MDPI AG, Sep. 01, 2021. doi: 10.3390/jmmp5030069.
- [87] N. Lashari, T. Ganat, S. Kalam, T. A. Chandio, T. Sharma, and S. Qureshi, "Impact of a novel HPAM/GO-SiO₂ nanocomposite on interfacial tension: Application for enhanced oil recovery," *Pet Sci Technol*, vol. 40, no. 3, pp. 290–309, Feb. 2022, doi: 10.1080/10916466.2021.1993915.
- [88] R. T. L. Ferreira, I. C. Amatte, T. A. Dutra, and D. Bürger, "Experimental characterization and micrography of 3D printed PLA and PLA reinforced with short carbon fibers," *Compos B Eng*, vol. 124, pp. 88–100, Sep. 2017, doi: 10.1016/j.compositesb.2017.05.013.
- [89] A. Plymill, R. Minneci, D. A. Greeley, J. Gritton, and D. Greeley, "Graphene and Carbon Nanotube PLA Composite Feedstock Graphene and Carbon Nanotube

PLA Composite Feedstock Development for Fused Deposition Modeling
Development for Fused Deposition Modeling Graphene and Carbon Nanotube
PLA Composite Feedstock Development for Fused Deposition Modeling.”
[Online]. Available: https://trace.tennessee.edu/utk_chanhonoproj/1955

- [90] N. Li, Y. Li, and S. Liu, “Rapid prototyping of continuous carbon fiber reinforced polylactic acid composites by 3D printing,” *J Mater Process Technol*, vol. 238, pp. 218–225, Dec. 2016, doi: 10.1016/j.jmatprotec.2016.07.025.
- [91] Q. Hu, Y. Duan, H. Zhang, D. Liu, B. Yan, and F. Peng, “Manufacturing and 3D printing of continuous carbon fiber prepreg filament,” *J Mater Sci*, vol. 53, no. 3, pp. 1887–1898, Feb. 2018, doi: 10.1007/s10853-017-1624-2.
- [92] C. Gonçalves, I. C. Gonçalves, F. D. Magalhães, and A. M. Pinto, “Poly(lactic acid) composites containing carbon-based nanomaterials: A review,” *Polymers (Basel)*, vol. 9, no. 7, pp. 1–37, 2017, doi: 10.3390/polym9070269.
- [93] E. Omanović-Miklićanin, A. Badnjević, A. Kazlagic, and M. Hajlovac, “Nanocomposites: a brief review,” *Health Technol (Berl)*, vol. 10, no. 1, pp. 51–59, Jan. 2020, doi: 10.1007/s12553-019-00380-x.
- [94] N. Vidakis, M. Petousis, K. Savvakis, A. Maniadi, and E. Koudoumas, “A comprehensive investigation of the mechanical behavior and the dielectrics of pure polylactic acid (PLA) and PLA with graphene (GnP) in fused deposition modeling (FDM),” *International Journal of Plastics Technology*, vol. 23, no. 2, pp. 195–206, 2019, doi: 10.1007/s12588-019-09248-1.

- [95] J. Bustillos, D. Montero, P. Nautiyal, A. Loganathan, B. Boesl, and A. Agarwal, “Integration of graphene in poly(lactic) acid by 3D printing to develop creep and wear-resistant hierarchical nanocomposites,” *Polym Compos*, vol. 39, no. 11, pp. 3877–3888, Nov. 2018, doi: 10.1002/pc.24422.
- [96] K. Prashantha and F. Roger, “Multifunctional properties of 3D printed poly(lactic acid)/graphene nanocomposites by fused deposition modeling,” *Journal of Macromolecular Science, Part A*, vol. 54, no. 1, pp. 24–29, Jan. 2017, doi: 10.1080/10601325.2017.1250311.
- [97] J. Butt, R. Bhaskar, and V. Mohaghegh, “Investigating the Influence of Material Extrusion Rates and Line Widths on FFF-Printed Graphene-Enhanced PLA,” *Journal of Manufacturing and Materials Processing*, vol. 6, no. 3, p. 57, 2022, doi: 10.3390/jmmp6030057.
- [98] S. Shi *et al.*, “Preparation of Highly Efficient Electromagnetic Interference Shielding Polylactic Acid/Graphene Nanocomposites for Fused Deposition Modeling Three-Dimensional Printing,” *Ind Eng Chem Res*, vol. 59, no. 35, pp. 15565–15575, Sep. 2020, doi: 10.1021/acs.iecr.0c02400.
- [99] J. C. Camargo, Á. R. Machado, E. C. Almeida, and E. F. M. S. Silva, “Mechanical properties of PLA-graphene filament for FDM 3D printing,” *The International Journal of Advanced Manufacturing Technology*, vol. 103, no. 5–8, pp. 2423–2443, Aug. 2019, doi: 10.1007/s00170-019-03532-5.
- [100] F. Daniel, N. H. Patoary, A. L. Moore, L. Weiss, and A. D. Radadia, “Temperature-dependent electrical resistance of conductive polylactic acid

- filament for fused deposition modeling,” *The International Journal of Advanced Manufacturing Technology*, vol. 99, no. 5–8, pp. 1215–1224, Nov. 2018, doi: 10.1007/s00170-018-2490-z.
- [101] E. Ivanov *et al.*, “PLA/Graphene/MWCNT Composites with Improved Electrical and Thermal Properties Suitable for FDM 3D Printing Applications,” *Applied Sciences*, vol. 9, no. 6, p. 1209, Mar. 2019, doi: 10.3390/app9061209.
- [102] F. Novotný, V. Urbanová, J. Plutnar, and M. Pumera, “Preserving Fine Structure Details and Dramatically Enhancing Electron Transfer Rates in Graphene 3D-Printed Electrodes via Thermal Annealing: Toward Nitroaromatic Explosives Sensing,” *ACS Appl Mater Interfaces*, vol. 11, no. 38, pp. 35371–35375, 2019, doi: 10.1021/acsami.9b06683.
- [103] G. Spinelli, R. Guarini, R. Kotsilkova, T. Batakliiev, E. Ivanov, and V. Romano, “Experimental and Simulation Studies of Temperature Effect on Thermophysical Properties of Graphene-Based Polylactic Acid,” *Materials*, vol. 15, no. 3, 2022, doi: 10.3390/ma15030986.
- [104] F. De Maio *et al.*, “3D-printed graphene polylactic acid devices resistant to SARS-CoV-2: Sunlight-mediated sterilization of additive manufactured objects,” *Carbon N Y*, vol. 194, pp. 34–41, 2022, doi: 10.1016/j.carbon.2022.03.036.
- [105] M. Á. Caminero, J. M. Chacón, E. García-Plaza, P. J. Núñez, J. M. Reverte, and J. P. Becar, “Additive manufacturing of PLA-based composites using fused filament fabrication: Effect of graphene nanoplatelet reinforcement on mechanical

- properties, dimensional accuracy and texture,” *Polymers (Basel)*, vol. 11, no. 5, 2019, doi: 10.3390/polym11050799.
- [106] T. Batakliiev *et al.*, “Nanoindentation analysis of 3D printed poly(lactic acid)-based composites reinforced with graphene and multiwall carbon nanotubes,” *J Appl Polym Sci*, vol. 136, no. 13, pp. 3–7, 2019, doi: 10.1002/app.47260.
- [107] S. Rostom and M. D. Dadmun, “Improving heat transfer in fused deposition modeling with graphene enhances inter filament bonding,” *Polym Chem*, vol. 10, no. 44, pp. 5967–5978, 2019, doi: 10.1039/c9py00832b.
- [108] V. Patravale, P. Dandekar, and R. Jain, “Characterization techniques for nanoparticulate carriers,” in *Nanoparticulate Drug Delivery*, Elsevier, 2012, pp. 87–121. doi: 10.1533/9781908818195.87.
- [109] S. Ebnesajjad, “Surface and Material Characterization Techniques,” in *Surface Treatment of Materials for Adhesion Bonding*, Elsevier, 2006, pp. 43–75. doi: 10.1016/B978-081551523-4.50006-7.
- [110] S. Villar-Rodil, Juan. I. Paredes, A. Martínez-Alonso, and Juan. M. D. Tascón, “Preparation of graphene dispersions and graphene-polymer composites in organic media,” *J Mater Chem*, vol. 19, no. 22, p. 3591, 2009, doi: 10.1039/b904935e.
- [111] T. Ramanathan *et al.*, “Functionalized graphene sheets for polymer nanocomposites,” *Nat Nanotechnol*, vol. 3, no. 6, pp. 327–331, Jun. 2008, doi: 10.1038/nnano.2008.96.

- [112] Y. Xu, W. Hong, H. Bai, C. Li, and G. Shi, “Strong and ductile poly(vinyl alcohol)/graphene oxide composite films with a layered structure,” *Carbon N Y*, vol. 47, no. 15, pp. 3538–3543, Dec. 2009, doi: 10.1016/j.carbon.2009.08.022.
- [113] Y. Shen *et al.*, “Chemical and thermal reduction of graphene oxide and its electrically conductive polylactic acid nanocomposites,” *Compos Sci Technol*, vol. 72, no. 12, pp. 1430–1435, Jul. 2012, doi: 10.1016/j.compscitech.2012.05.018.
- [114] J. Drzeżdżon, D. Jacewicz, A. Sielicka, and L. Chmurzyński, “Characterization of polymers based on differential scanning calorimetry based techniques,” *TrAC Trends in Analytical Chemistry*, vol. 110, pp. 51–56, Jan. 2019, doi: 10.1016/j.trac.2018.10.037.
- [115] E. Tarani, A. Wurm, C. Schick, D. N. Bikiaris, K. Chrissafis, and G. Vourlias, “Effect of graphene nanoplatelets diameter on non-isothermal crystallization kinetics and melting behavior of high density polyethylene nanocomposites,” *Thermochim Acta*, vol. 643, pp. 94–103, Nov. 2016, doi: 10.1016/j.tca.2016.09.018.
- [116] S. Banerjee, A. K. Nayak, and K. K. Sen, “Aquasomes: a nanoparticulate approach for therapeutic applications,” in *Systems of Nanovesicular Drug Delivery*, Elsevier, 2022, pp. 207–219. doi: 10.1016/B978-0-323-91864-0.00025-5.
- [117] L. McKeen, “Introduction to the Physical, Mechanical, and Thermal Properties of Plastics and Elastomers,” in *The Effect of Sterilization on Plastics and Elastomers*, Elsevier, 2012, pp. 57–84. doi: 10.1016/B978-1-4557-2598-4.00003-4.

- [118] K. Kawakami, "Pharmaceutical Applications of Thermal Analysis," 2018, pp. 613–641. doi: 10.1016/B978-0-444-64062-8.00009-7.
- [119] V. Abhilash, N. Rajender, and K. Suresh, "X-ray diffraction spectroscopy of polymer nanocomposites," in *Spectroscopy of Polymer Nanocomposites*, Elsevier, 2016, pp. 410–451. doi: 10.1016/B978-0-323-40183-8.00014-8.
- [120] S. R. Laraba *et al.*, "Enhancing Structural and Thermal Properties of Poly(lactic acid) Using Graphene Oxide Filler and Anionic Surfactant Treatment," *Molecules*, vol. 28, no. 18, Sep. 2023, doi: 10.3390/molecules28186442.
- [121] T. Tábi, S. Hajba, and J. G. Kovács, "Effect of crystalline forms (α' and α) of poly(lactic acid) on its mechanical, thermo-mechanical, heat deflection temperature and creep properties," *Eur Polym J*, vol. 82, pp. 232–243, Sep. 2016, doi: 10.1016/j.eurpolymj.2016.07.024.
- [122] N. N. Daéid, "FORENSIC SCIENCES | Systematic Drug Identification," in *Encyclopedia of Analytical Science*, Elsevier, 2005, pp. 471–480. doi: 10.1016/B0-12-369397-7/00197-7.
- [123] M. Tanase-Opedal, E. Espinosa, A. Rodríguez, and G. Chinga-Carrasco, "Lignin: A Biopolymer from Forestry Biomass for Biocomposites and 3D Printing," *Materials*, vol. 12, no. 18, p. 3006, Sep. 2019, doi: 10.3390/ma12183006.
- [124] R. Al-Itry, K. Lamnawar, and A. Maazouz, "Reactive extrusion of PLA, PBAT with a multi-functional epoxide: Physico-chemical and rheological properties,"

- Eur Polym J*, vol. 58, pp. 90–102, Sep. 2014, doi:
10.1016/j.eurpolymj.2014.06.013.
- [125] S. Knop, T. L. C. Jansen, J. Lindner, and P. Vöhringer, “On the nature of OH-stretching vibrations in hydrogen-bonded chains: Pump frequency dependent vibrational lifetime,” *Physical Chemistry Chemical Physics*, vol. 13, no. 10, p. 4641, 2011, doi: 10.1039/c0cp02143a.
- [126] R. Roy *et al.*, “Role of oxygen functionality on the band structure evolution and conductance of reduced graphene oxide,” *Chem Phys Lett*, vol. 677, pp. 80–86, Jun. 2017, doi: 10.1016/j.cplett.2017.03.079.
- [127] T. S. Vo and T. T. B. C. Vo, “Organic dye removal and recycling performances of graphene oxide-coated biopolymer sponge,” *Progress in Natural Science: Materials International*, vol. 32, no. 5, pp. 634–642, Oct. 2022, doi: 10.1016/j.pnsc.2022.05.004.
- [128] N. Saba, M. Jawaid, and M. T. H. Sultan, “An overview of mechanical and physical testing of composite materials,” in *Mechanical and Physical Testing of Biocomposites, Fibre-Reinforced Composites and Hybrid Composites*, Elsevier, 2019, pp. 1–12. doi: 10.1016/B978-0-08-102292-4.00001-1.
- [129] Y. Zhao, Y. Chen, and Y. Zhou, “Novel mechanical models of tensile strength and elastic property of FDM AM PLA materials: Experimental and theoretical analyses,” *Mater Des*, vol. 181, p. 108089, 2019, doi: 10.1016/j.matdes.2019.108089.

- [130] L. Yang, S. Li, Y. Li, M. Yang, and Q. Yuan, “Experimental Investigations for Optimizing the Extrusion Parameters on FDM PLA Printed Parts,” *J Mater Eng Perform*, vol. 28, no. 1, pp. 169–182, 2019, doi: 10.1007/s11665-018-3784-x.
- [131] D. Verma, P. C. Gope, A. Shandilya, and A. Gupta, “Mechanical-Thermal-Electrical and Morphological Properties of Graphene Reinforced Polymer Composites: A Review,” *Transactions of the Indian Institute of Metals*, vol. 67, no. 6, pp. 803–816, Dec. 2014, doi: 10.1007/s12666-014-0408-5.
- [132] J. Liang *et al.*, “Molecular-Level Dispersion of Graphene into Poly(vinyl alcohol) and Effective Reinforcement of their Nanocomposites,” *Adv Funct Mater*, vol. 19, no. 14, pp. 2297–2302, Jul. 2009, doi: 10.1002/adfm.200801776.
- [133] M. Jafarkhani, Z. Salehi, and T. Nematian, “Preparation and characterization of chitosan/graphene oxide composite hydrogels for nerve tissue Engineering,” *Mater Today Proc*, vol. 5, no. 7, pp. 15620–15628, 2018, doi: 10.1016/j.matpr.2018.04.171.
- [134] L. Jiang, X. Shen, J. Wu, and K. Shen, “Preparation and characterization of graphene/poly(vinyl alcohol) nanocomposites,” *J Appl Polym Sci*, vol. 118, no. 1, pp. 275–279, Oct. 2010, doi: 10.1002/app.32278.
- [135] S. R. Djafari Petroudy, “Physical and mechanical properties of natural fibers,” in *Advanced High Strength Natural Fibre Composites in Construction*, Elsevier, 2017, pp. 59–83. doi: 10.1016/B978-0-08-100411-1.00003-0.

- [136] P. Larour, J. Freudenthaler, and T. Weissböck, “Reduction of cross section area at fracture in tensile test: measurement and applications for flat sheet steels,” *J Phys Conf Ser*, vol. 896, p. 012073, Sep. 2017, doi: 10.1088/1742-6596/896/1/012073.
- [137] A. Shrivastava, “Plastic Properties and Testing,” in *Introduction to Plastics Engineering*, Elsevier, 2018, pp. 49–110. doi: 10.1016/B978-0-323-39500-7.00003-4.
- [138] B. C. Chakraborty and D. Ratna, “Experimental techniques and instruments for vibration damping,” in *Polymers for Vibration Damping Applications*, Elsevier, 2020, pp. 281–325. doi: 10.1016/B978-0-12-819252-8.00006-9.
- [139] J. Luo, H. Wang, D. Zuo, A. Ji, and Y. Liu, “Research on the Application of MWCNTs/PLA Composite Material in the Manufacturing of Conductive Composite Products in 3D Printing,” *Micromachines (Basel)*, vol. 9, no. 12, p. 635, Nov. 2018, doi: 10.3390/mi9120635.
- [140] T. Kobayashi, “Impact Testing,” in *Encyclopedia of Materials: Science and Technology*, Elsevier, 2001, pp. 4027–4031. doi: 10.1016/B0-08-043152-6/00707-5.
- [141] E. A. Campo, “Physical Properties of Polymeric Materials,” in *Selection of Polymeric Materials*, Elsevier, 2008, pp. 175–203. doi: 10.1016/B978-081551551-7.50007-3.

- [142] M. Wang and C. Wang, “Bulk Properties of Biomaterials and Testing Techniques,” in *Encyclopedia of Biomedical Engineering*, Elsevier, 2019, pp. 53–64. doi: 10.1016/B978-0-12-801238-3.99861-1.

VITAE

Name :Tarig Yassin Makki

Nationality :Serbian

Date of Birth :3/13/1999

Email :tarigmamdouh@hotmail.co.uk

Address :Kanarevo brdo, 12v, Belgrade, Serbia, 11090

Academic Background :B.S. in Mechanical Engineering 2019 (Eastern Mediterranean University, Northern Cyprus)

Skills

- Computer Skills (SolidWorks, Cura ,Microsoft Office {Word, Excel, PowerPoint}).
- Additive Manufacturing
- Plastic processing technologies
- Material Characterizations
- Composites
- Technical writing and public speaking